Two transcriptionally distinct pathways drive female development in a reptile with both genetic and temperature dependent sex determination

Sarah L. Whiteley[1,2], Clare E. Holleley[2], Susan Wagner[1], James Blackburn[3,4], Ira W. Deveson[3,4], Jennifer A. Marshall Graves[1,5], Arthur Georges[1*]

Institutional Affiliations

[1]Institute for Applied Ecology, University of Canberra, Australia

[2] Australian National Wildlife Collection CSIRO National Research Collections Australia, Canberra, Australia

[3]Garvan Institute of Medical Research, Sydney, Australia

[4] St. Vincent's Clinical School, UNSW, Sydney, Australia

[5] Latrobe University, Melbourne, Australia.

*Corresponding author: georges@aerg.canberra.edu.au, Ph: +61 418866741

Abstract

How temperature determines sex remains unknown. A recent hypothesis proposes that conserved cellular mechanisms (calcium and redox; 'CaRe' status) sense temperature and identify genes and regulatory pathways likely to be involved in driving sexual development. We take advantage of the unique sex determining system of the model organism, *Pogona vitticeps,* to assess predictions of this hypothesis. *P. vitticeps* has ZZ male: ZW female sex chromosomes whose influence can be overridden in genetic males by high temperatures, causing male-to-female sex reversal. We compare a developmental transcriptome series of ZWf females and temperature sex reversed ZZf females. We demonstrate that early developmental cascades differ dramatically between genetically driven and thermally driven females, later converging to produce a common outcome (ovaries). We show that genes proposed as regulators of thermosensitive sex determination play a role in temperature sex reversal. Our study greatly advances the search for the mechanisms by which temperature determines sex.

Author Summary

In many reptiles and fish, environment can determine, or influence, the sex of developing embryos. How this happens at a molecular level that has eluded resolution for half a century of intensive research. We studied the bearded dragon, a lizard that has sex chromosomes (ZZ male and ZW female), but in which that temperature can override ZZ sex chromosomes to cause male to female sex reversal. This provides an unparalleled opportunity to disentangle, in the same species, the biochemical pathways required to make a female by these two different routes. We sequenced the transcriptomes of gonads from developing ZZ reversed and normal ZW dragon embryos and discovered that different sets of genes are active in ovary development driven by genotype or temperature. Females whose sex was initiated by temperature showed a transcriptional profile consistent with the recently-proposed Calcium-Redox hypotheses of cellular temperature sensing. These findings are an important for understanding how the environment influences the development of sex, and more generally how the environment can epigenetically modify the action of genes.

Key words

Sex reversal, gonad differentiation, thermosensitivity, calcium signalling, oxidative stress

Introduction

Sex determination in vertebrates may be genetic or environmental. In genetic sex determination (GSD), offspring sex is determined by sex chromosomes inherited from each parent, which bear either a dominant gene on the heteromorphic sex chromosome (as with *SRY* in humans) (1,2), or a dosage sensitive gene on the homomorphic sex chromosome (as with *DMRT1* in birds) (3). However, some fish and many reptile species exhibit environmental sex determination (ESD), whereby a variety of external stimuli can determine sex, most commonly involving temperature (temperature dependent sex determination, TSD) (4,5). While GSD and ESD are commonly viewed as a dichotomy, the reality is far more complex. Sex determination in vertebrates exists as a continuum of genetic and environmental influences (6) whereby genes and environment can interact to determine sex (7–9).

The genetic mechanisms that act in highly conserved pathways that ultimately yield testes or ovaries are quite well characterised (5,10,11). Yet, despite decades of research on ESD systems, and TSD in particular, the upstream mechanisms by which an external signal is transduced to determine sex remains unknown (12). Recent research led to the hypothesis that the cellular sensor initiating ESD is controlled by the balance of redox regulation and calcium (Ca^{2+}) signalling (CaRe) (13). The CaRe hypothesis proposes a link between CaRe sensitive cellular signalling and the highly conserved epigenetic processes that have been implicated in thermolabile sex (TSD and temperature sex reversal) (12,14–17). The CaRe hypothesis posits that in ESD systems a change in intracellular Ca^{2+} (probably mediated by thermosensitive transient receptor potential TRP channels) and increased reactive oxygen species (ROS) levels caused by high temperatures, alter the CaRe status of the cell, triggering cellular signalling cascades that drive differential sex-specific expression of genes to determine sex. The CaRe hypothesis makes several testable predictions for how an environmental signal is captured and transduced by the gonadal cells to deliver a male or a female phenotype.

Species in which genes and environment both influence sex determination provide unique opportunities to directly compare the regulatory and developmental processes involved in sex determination. By early gonad differentiation directed by genotype and temperature, it is possible to assess predictions of the CaRe hypothesis. In our model species, the central bearded dragon (*Pogona vitticeps*), we can compare female development via thermal and genetic cues because extreme temperatures (>32˚C) override the male sex-determining signal from the ZZ sex micro-chromosomes to feminise embryos (8,18). This makes it possible to distinguish between the previously confounded effects of thermal stress and phenotypic sex by comparing gene expression throughout embryonic development in sex reversed ZZf females with genetic ZWf females.

We can explore the predictions of the CaRe model, namely that under sex-reversing conditions, we will see differential regulation of: 1) genes involved in responding to Ca^{2+} influx and signalling; 2) genes involved in antioxidant and/or oxidative stress responses; 3) genes with known thermosensitivity, such as heat shock proteins; 4) candidate TSD genes, such as *CIRBP* and Jumonji family genes; 5) signal transduction pathways such as the JAK-STAT and NF-κB pathways.

We compared gene expression profiles in *P. vitticeps* embryonic gonads at three developmental stages (6, 12 and 15; 19,20) for ZWf and ZZf eggs incubated at 28°C and 36°C respectively (Fig. 1). This allowed us to compare drivers of sex determination and differentiation under genetic or thermal influence. We found that very different regulatory processes are involved in temperature-driven regulation compared to gene-driven regulation, although both lead to a conserved outcome (ovaries, Fig. 2). We discovered dramatic changes in cellular calcium homeostasis in the gonads of ZZf individuals incubated at high sex reversing temperatures, which fulfill predictions of the CaRe hypothesis that this is the key driver of temperature induced feminization. We argue that differential expression of calcium channels, and subsequent alterations of the intracellular environment combined with increased ROS production encode, then transduce, the thermal signal into altered gene expression, ultimately triggering male to female sex reversal in *P. vitticeps*.

Results

Gene-driven female determination in ZWf embryos

Comparisons between stages in ZWf embryos (Fig. 3B, Fig. S1, Additional file S1) showed that many genes were differentially expressed between stages 6 and 12 (210 genes downregulated and 627 genes upregulated at stage 12), but few genes were differentially expressed between stages 12 and 15 (2 genes upregulated at stage 15).

SOX9 and *GADD45G*, genes strongly associated with male development in mammals, were downregulated from stage 6 to stage 12, whereas various female related genes were upregulated, such as *PGR*, *ESR2*, *CYP19A1,* and *CYP17A1*. *BMP7,* a regulator of germ cell proliferation was upregulated at stage 12 (21), as were components of the NOTCH signalling pathway (*JAG2*, *DLL3, DLL4*), which are required for the suppression of Leydig cell differentiation (22,23). *SRD5A2*, whose product catalyses the 5-α reduction of steroid hormones such as testosterone and progesterone, was also upregulated (24,25).

Notably, there was little differential expression between stages 12 and 15, suggesting that genetically driven ovarian development is complete by stage 12 (Additional file S1).

Temperature-driven female determination in ZZf embryos

Differential expression analysis of temperature-driven female development in ZZf embryos revealed many genes are differentially expressed between stages 6 and 12 (297 downregulated and 511 upregulated at stage 12) and no genes are differentially expressed between stage 12 and 15 (Fig. 3, Fig. S1, Additional file S1), suggesting completion of the ovarian development by stage 12 also in ZZf females.

Upregulation of *FZD1*, a receptor for *Wnt* family proteins required for female development, suggests the activity of female pathways in ZZf embryos (26). As was seen for ZWf females, canonical NOTCH ligands *DLL3* and *DLL4* were upregulated from stage 6 to stage 12 in ZZf females. However, this did not coincide with upregulation of JAG ligands or NOTCH genes, and the GO term “negative regulation of NOTCH signalling” was enriched within the group of genes upregulated from stage 6 to 12 in ZZf females (Additional file S2). Further, *PDGFB*, which is required for Leydig cell differentiation, was upregulated (27).

Together, this suggests that the NOTCH signalling pathway may not be activated, and Leydig cell recruitment is not strongly repressed at stage 12 in ZZf. Alternatively, the absence of NOTCH signalling may indicate an important transition from progenitor cells to differentiated gonadal cell types in the early stages of the developing ovary (28). These apparent differences in NOTCH signalling between ZZf and ZWf embryos suggests that ovarian development has progressed further in ZWf females.

Interestingly, genes typically associated with male development show diverse regulation in ZZf embryos, with some being downregulated and some being upregulated from stage 6 to 12. These included *WNT5a* and *SFRP2,* which are both involved in testicular development in mice (29,30), *NCOA4*, which enhances activity of various hormone receptors, and exhibits high expression in testes in mice during development (31), and *HSD17B3*, which catalyses androstenedione to testosterone (32). Unlike what was observed in ZWf embryos, *SOX9* and *GADD45G* were not differentially expressed between stages 6 and 12 in ZZf embryos. *TGFBR3L*, which is required for Leydig cell function in mouse testis (33), and *NR5A1*, *SOX4,* and *AMHR2* (34–37) were also differentially expressed between stages 6 and 12 (Additional file S1).

A suite of genes typically associated with female development were upregulated from stage 6 to 12 (38), for example, *FOXL2*, *CYP17A1, RSPO1,* and *ESRRG*. As was also observed in stage 12 ZWfs, *ESR2, BMP7*, *CYP19A1,* and *PGR,* were more highly expressed at stage 12 in ZZfs. Notably, *CYP19A1* was much more strongly upregulated at stage 12 in ZZfs compared with stage 12 in ZWfs (Additional file S1). The increase in sex specific genes was also reflected in enriched GO terms at stage 12, which included “hormone binding”, “steroid hormone receptor activity”, and “female sex determination” (Additional file S2).

Ovarian maintenance in sex reversed ZZf females

The maintenance of female gene expression and ovarian development at stage 12 in ZZf females may be centrally mediated by *STAT4* (Fig. 4). As a member of the *JAK-STAT* pathway, *STAT4* is transduced by various signals, including reactive oxygen species, to undergo phosphorylation and translocate from the cytoplasm to nucleus (39–41). At stage 12, *STAT4* is upregulated, alongside *PDGFB* compared to stage 6 in ZZf females. *PDGFB* is known to activate *STAT4* (40). Various *STAT4* target genes, notably *AMHR2*, *NR5A1*, *EGR1,*

and *KDM6B* (40) are also upregulated at stage 12 (Additional file S1). Consistent with this link is the observation that a member of the same gene family, *STAT3,* is implicated in TSD in *Trachemys scripta* (17).

Several targets of *STAT4* are upregulated at stage 12, including *AMHR2* and *NR5A1*. Though typically associated with male development, *AMHR2* and *NR5A1* may also have roles in ovarian development. Although it is the primary receptor for *AMH*, *AMHR2* exhibits considerable evolutionary flexibility is sometimes associated with ovarian development (reviewed by (36)). *NR5A1* is also often associated with male development, as it positively regulates expression of *AMH* and *SOX9* in mammals (42). However, *NR5A1* can also interact with *FOXL2* and bind to *CYP19A1* promoter to promote female development (43,44). The upregulation of *FOXL2* and *CYP19A1,* but not *AMH* or *SOX9,* suggests that *NR5A1* is involved in the establishment of the ovarian pathway in ZZf females.

EGR1 positively regulates *DMRT1* expression through promoter binding in Sertoli cells, but knock-out of this gene can also cause female infertility in mice (45–47). EGR1 is also associated with female development in birds, likely controlling the production of steroid hormones (34). As was observed for *NR5A1*, *DMRT1* was also lowly expressed, suggesting it is not activated by *EGR1* in ZZf females.

One explanation for these expression trends is that male-associated genes are not strongly repressed at this stage during the sex reversal process, and that more prolonged exposure to the sex reversing temperature is required to firmly establish the female phenotype. However, we argue that the results more strongly suggest ROS-induced activation of *STAT4*, and subsequent phosphorylation and translocation, probably mediated by *PDGFB*, allows for the transcriptional activation of *NR5A1, AMHR2,* and *EGR1*, which in the temperature driven process of sex reversal in the ZZf embryos serve to maintain the ovarian phenotype.

Differential regulation of female developmental pathways

To better understand differences in ovarian developmental pathways, we compared gene expression of ZZf with ZWf embryos at each developmental stage. There are large gene expression differences between normal ZWf females and ZZf sex reversed females early in

development, before the bipotential gonad differentiates into an ovary. These differences are most pronounced early in development and diminish as development progresses. Stage 6 had the largest number of differentially expressed genes (DEGs) (281 genes higher expressed in ZWf embryos, 423 genes higher expressed in ZZf), with fewer DEGs at stage 12 (51 genes upregulated in ZWf, 63 genes upregulated in ZZf), and fewest at stage 15 (1 gene upregulated in ZWf, 2 genes upregulated in ZZf) (Fig. 3B, Additional file S3, Fig. S1). This suggests that the sex reversed embryos start out on a male developmental trajectory, which they pursue beyond the thermal cue (3 days when the eggs were switched to high incubation temperatures, Fig. 1), but by stage 12 development has been taken over by female genes.

Gene ontology (GO) enrichment analysis showed important differences between ZZf and ZWf at stage 6, and provides independent support for the role of calcium and redox regulation in ZZf females as proposed by the CaRe model (Fig. 5 A-D, Additional file S4). GO processes enriched in the gene set higher expressed in ZZf at stage 6 included “oxidation-reduction processes”, “cytosolic calcium ion transport”, and “cellular homeostasis” (Fig. 5A, Additional file S4). GO function enrichment also included several terms related to oxidoreductase activities, as well as “active transmembrane transporter activity” (Fig. 5C, Additional file S4). No such GO terms were enriched in the gene set higher expressed in ZWf. Instead, enriched GO terms included “anatomical structure development”, and “positive regulation of developmental growth” (Fig. 5B, D, Additional file S4).

Genes involved in female sex differentiation were higher expressed at stage 6 in normal ZWf embryos compared to sex reversed ZZf embryos (Additional file S3). These included *FOXL2*, *ESR2*, *PGR*, and *GATA6* (48,49). Higher expression of *LHX9*, a gene with a role in bipotential gonad formation in mammals and birds, was more highly expressed in ZWf embryos (42,50–52). Two genes with well described roles in male development, *SOX4* and *ALDH1A2* (53–55), were also higher expressed in ZWf embryos, suggesting they have an as yet unknown function in the early establishment of the ovarian trajectory in *P. vitticeps*.

Taken together, these results further suggest that ZWf females are committed to the female pathway earlier than ZZf females. This is not surprising, since ZWf females possess sex chromosomes from fertilisation, whereas ZZf individuals have had only 3 days of exposure to a sex reversal inducing incubation temperature (Fig. 1A). This data is the first to

247 demonstrate a difference in timing of genetic signals between gene and temperature driven
248 development in the same species.

249 Three genes were constantly differentially expressed between ZWf and ZZf embryos at
250 all three developmental stages (Fig. 3A). *GCA* (grancalcin) was upregulated in ZWf embryos,
251 and *KDM6B* and *CIRBP* were upregulated in ZZf embryos at all developmental stages. *GCA* is
252 a calcium binding protein commonly found in neutrophils and is associated with the Nf-κB
253 pathway (56,57). It has no known roles in sex determination, but its consistent upregulation
254 in ZWf embryos compared to ZZf embryos suggests *GCA* is associated with gene driven
255 ovarian development, at least in *P. vitticeps*.

256 Further analysis of gene expression trends using K-means clustering analysis (58) was
257 used to investigate genes associated with female development, and to determine to what
258 extent these genes are shared between ZZf and ZWf embryos (Fig. 6, Additional file S5).
259 Clusters with upward trends reflect genes likely to be associated with female development,
260 so clusters 1 and 4 in ZWf (ZWC1 and ZWC4), and clusters 1 and 2 in ZZf (ZZC1 and ZZC2),
261 were explored in greater detail (Fig. 6, Additional file S5).

262 ZWC4 and ZZC2 shared 374 genes. Enriched GO terms included "germ cell
263 development" and "reproductive processes" (Additional file S6), consistent with a link with
264 female development. Genes identified included *FIGLA*, a gene known to regulate oocyte-
265 specific genes in the female mammalian sex determination pathway (59), and *STRA8* which
266 controls entry of oocytes into meiosis. Intriguingly, the GO term "spermatid development"
267 was also enriched, encompassing many genes with known roles in testes function, including
268 *ADAD1* and *UBE2J1* (60,61). This suggests that genes involved in male sex determination in
269 mammals may have been co-opted for use in the ovarian pathway in reptiles, so their roles
270 require further investigation in other vertebrate groups, particularly given the complex
271 nature of gene expression in sperm cell types.

272 ZWC1 and ZZC1 shared 998 genes. ZZC1 has about 700 unique genes and ZWC1 about
273 500. GO analysis on shared genes between these clusters (n = 998) revealed enrichment
274 terms such as "kinase binding" and "intracellular signal transduction" (Additional file S5).
275 Genes unique to ZZC1 included members of heat shock protein families (*HSPB11, HSPA4,*
276 *HSP90AB1, HSPH1, HSPB1, HSPD1*), heterogenous ribonucleoprotein particles (*HNRNPUL1*),

277 mitogen activated proteins (including *MAPK1, MAPK9, MAP3K8*), and chromatin
278 remodelling genes (*KDM2B, KDM1A, KDM5B, KDM3B*). GO enrichment for genes unique to
279 ZZC1 included "mitochondrion organisation", "cellular localisation", and "ion binding", while
280 GO enrichment for genes unique to ZWC1 included "regulation of hormone levels" and
281 numerous signalling related functions (Additional file S6).

282 Taken together, our results show that although the same ovarian phenotype is
283 produced in genetic and temperature induced females, this end is achieved via different
284 gene expression networks. This is most pronounced at stage 6, after which the extent of the
285 differences decreases through development. This reflects canalisation of the gonadal fate to
286 a shared outcome (ovaries, Fig. 2).

287 *Signature of hormonal and cellular stress in ZWf females*

288 Previous work on *P. vitticeps* has shown a more than 50-fold upregulation of a hormonal
289 stress response gene, *POMC,* in sex reversed adult females, leading to the suggestion that
290 induction of sex reversal is in response to temperature stress, or that it is an inherently
291 stressful event, the effects of which persist into adult life (14). We therefore investigated
292 the expression of stress related genes in ZZf and ZWf embryos.

293 We found considerable evidence that ZZf embryos experience oxidative stress, likely
294 resulting from increased ROS production (discussed in detail below). However, contrary to
295 our expectations, we found that ZWf embryos showed higher expression than ZZf of
296 hormonal stress genes and pathways that have been hypothesized to be involved in sex
297 reversal (Fig. 5E-F, Additional file S3). Genes upregulated in ZWf embryos compared to ZZf
298 embryos included *STAT1*, a component of the JAK-STAT pathway, with several roles in stress
299 responses (62), and *MAP3K1* and *MAPK8*, which are typically involved in mediating stress-
300 related signal transduction cascades (63–65). *TERF2IP* is also upregulated; this gene is
301 involved in telomere length maintenance and transcription regulation (66). When
302 cytoplasmic, *TERF2IP* associates with the I-kappa-B-kinase (IKK) complex and promotes IKK-
303 mediated phosphorylation of RELA/p65, activating the NF-κB pathway and increasing
304 expression of its target genes (67). Notably two members of the IKK complex, *IKBKG* (also
305 known as *NEMO*) and *PRKCI*, which are involved in NF-κB induction, were also upregulated
306 in ZWf embryos compared to ZZf embryos (Fig. 4b), implying activation of the NF-κB

pathway (68). This pathway is typically associated with transducing external environmental signals to a cellular response (69,70), but also has diverse roles in sex determination in mammals, fish, and invertebrate models (reviewed by Castelli *et al.*, 2019).

CRH, another gene upregulated at stage 6 in ZWf females compared with ZZf females (Fig. 5b, supplementary file S3), is best known for its role as a neuropeptide synthesised in the brain in response to stresses that trigger the hypothalamic-pituitary-adrenal (HPA) axis (71,72). The role of *CRH* production in the gonads, particularly in ovaries is currently poorly understood (73–76). High *CRH* expression in ZWf gonads is the first observation of this in reptiles. The role of the hormonal stress response during embryonic development, and its apparent discordance with results observed in adults in *P. vitticeps* requires further investigation (14).

Cellular signalling cascades driving sex reversal

Results of this study provide considerable corroborative support for the CaRe model, which proposes a central role for calcium and redox in sensing and transducing environmental signals to determine sex. Many of the genes and pathways predicted by the CaRe model to be involved in sex reversal were shown to be upregulated in ZZf embryos at stage 6 compared to ZWf embryos. We use the CaRe model as a framework to understand the roles of each signalling participant in their cellular context during the initiation of sex reversal (Fig. 7). This interpretation is also independently supported by GO analysis, showing enrichment of expected terms, such as “cytosolic calcium ion transport” (Additional file S4), as well as k-means clustering analysis (Additional files S4, S5).

Cluster 6 in ZZf (Fig. 6A) shows genes whose expression decreases after stage 6, so is likely to include genes responsible for the initial response to temperature and initiation of sex reversal, whose continuing action is not required once the ovarian trajectory has been established. Consistent with this assumption, as well as with predictions from the CaRe model, the 4050 genes in this cluster were enriched for GO terms that included “oxidation-reduction process” and various oxidoreductase activities (Additional files S5, S6).

Calcium transport, signalling, and homeostasis

Our data suggest that exposure to high temperatures may cause a rapid increase in cytosolic Ca^{2+} concentrations, as calcium influx is probably mediated by the thermosensitive calcium channel, *TRPV2* (77,78). *TRPV2* was upregulated in stage 6 ZZf embryos compared to ZWf embryos (Fig. 6). Transient receptor potential (TRP) ion channels, including *TRPV2,* have previously been implicated in TSD in *Alligator sinensis* and *A. mississippiensis*, as well as the turtle *Trachemys scripta* (79–82).

TRPV2 mediated Ca^{2+} influx may trigger a cascade of changes within the gonadal cells of ZZf females, which restore calcium homeostasis, critical to avoid apoptosis (83,84). We observed evidence of such a homeostatic response, with the upregulation of seven genes involved in Ca^{2+} transport and sequestration in ZZf females compared to ZWf females at stage 6 (Fig. 6). Specifically, *MCU*, *ATP2B1*, *ATP2B4*, together regulate calcium homeostasis through active transport of calcium into the mitochondria and into the extracellular space (85–87). *KCNN1* and *CACNB3* encode proteins required for the formation of plasma membrane channels controlling the passage of Ca^{2+} (88–90). *CACNB3* and *KCNN1* have well characterised roles in the nervous system, and excitable cell types in muscle, but their association with TSD in embryonic gonads is novel (88,89). Evidence is also building for a broader role for voltage-gated calcium channels, including *CACNB3*, in orchestrating Ca^{2+} signalling and gene regulation (91). We suggest that *KCNN1* and *CACNB3* in gonads of TSD species play roles in mediating the homeostatic response to elevated cytosolic Ca^{2+} concentrations, and are involved in the subsequent modulation of Ca^{2+} signalling pathways.

TRPC4, another TRP family gene was, upregulated in stage 12 compared to stage 6 in both ZZf and ZWf embryos. *TRPC4* is expressed in mouse sperm and inhibited by progesterone (92,93) but has no known association with sex determination. *TRPC4* belongs to the TRPC superfamily, which all conduct calcium ions into the cell, typically through phospholipase C and calmodulin signalling pathways, G-protein-coupled receptors, and receptor tyrosine kinases (94,95). Notably, *PLCL2* a phospholipase gene, together with calmodulin genes *CALM1* and *CAMKK1*, were upregulated alongside *TRPC4* from stage 6 to stage 12 in ZZf embryos but not in ZWf embryos (Additional file S3). Given *TRPC4* is upregulated from stage 6 to 12 in both ZZf and ZWf females, it may play a more conserved role in ovarian development in *P. vitticeps*.

Several genes with functions in calcium metabolism were upregulated in stage 6 ZZf embryos compared to stage 6 ZWf embryos. *CALR* encodes a multifunctional protein that acts as a calcium binding storage protein in the lumen of the endoplasmic reticulum, so is also important for regulating Ca^{2+} homeostasis (84,96,97). *CALR* is also present in the nucleus, where it may play a role in regulation of transcription factors, notably by interacting with DNA-binding domains of glucocorticoid and hormone receptors, inhibiting the action of androgens and retinoic acid (97–101). *TMEM38B* (commonly known as *TRICB*) is also found on the endoplasmic and sarcoplasmic reticula, where it is responsible for regulating the release of Ca^{2+} stores in response to changes in intracellular conditions (102).

MCU, ATP2B1, ATP2B4, KCNN1, CACNB3, CALR, and *TMEM38B* have no known roles in vertebrate sex determination, so their association with sex reversal in *P. vitticeps* is new. This upregulation during the early stage of sex reversal suggests that they are upstream modulators involved in the transduction of environmental cues that trigger sex determination cascades, which is consistent with predictions made by the CaRe hypothesis.

We hypothesize that intracellular Ca^{2+} increases in stage 6 ZZf gonads, and further observe that Ca^{2+} signalling related genes are also upregulated in ZZf females compared to stage 6 ZWf females (Fig. 7). *C2CD2* and *C2CD2L* are both thought to be involved in Ca^{2+} signalling, although there is no functional information about these genes. Of note is the significant upregulation of *S100Z*, which is a member of a large group of EF-hand Ca^{2+} binding proteins that play a role in mediating Ca^{2+} signalling (103). The EF-hand domain is responsible for binding Ca^{2+}, allowing proteins like that encoded by *S100Z* to 'decode' the Ca^{2+} biochemical signal and translate this to various targets involved in many cellular functions including Ca^{2+} buffering, transport, and enzyme activation (104,105). *PLCB1* also contains an EF-hand binding domain and behaves similarly, being activated by many extracellular stimuli and effecting numerous signalling cascades. It can translocate to the plasma membrane and nucleus, and release Ca^{2+} from intracellular stores (106). Some Ca^{2+} related genes (*GCA* and *CALM1*) are also upregulated in ZWf embryos, but make only a small proportion of the overall response in differential gene expression (Additional file S3).

Oxidative stress in response to high temperatures

The upregulation of antioxidant genes in ZZf compared to ZWf embryos suggests that the gonadal cells in the ZZf embryos are in a state of oxidative stress (Fig. 7). As was proposed by the CaRe model, we see results consistent with the prediction that high incubation temperatures increase metabolism, which increases the production of reactive oxygen species (ROS) by the mitochondria, resulting in oxidative stress (13). ROS are required for proper cellular function, but above an optimal threshold, they can cause cellular damage (107,108). Crossing this threshold launches the antioxidant response, which causes the upregulation of antioxidant genes to produce protein products capable of neutralising ROS (109,110). We observed upregulation of redox related genes, specifically of *TXNDC11*, *PRDX3*, *MGST1* in ZZf embryos compared to ZWf embryos at stage 6. Also upregulated was *FOXO3*, which plays a role in oxidative stress responses, typically by mediating pro-apoptotic cascades (111,112). Importantly, antioxidants play other cellular roles besides neutralisation of ROS. One of these is the alteration of cysteine resides through a process known as S-glutathionylation (113).

Various redox related genes were downregulated from stage 6 to 12 in ZZf embryos but not in ZW embryos, including *GLRX* and *PRDX3* (114), as well as numerous genes involved in ROS induced DNA damage repair; *LIG4, ENDOD1,* and *HERC2* (115). This indicates a need for expression of these genes specifically in ZZf embryos in early stages that ceases in transition to stage 12. *STAT4*, a member of the ROS-induced JAK-STAT pathway (Simon et al. 1998), and *DDIT4*, which is involved stress responses to DNA damage (116), were both upregulated from stage 6 to stage 12 in ZZf embryos.

The vertebrate antioxidant response is typically initiated by *NRF2*, but we observed no differential expression of *NRF2*, only upregulation of some of its known targets in ZZf embryos (117). This may mean that the action of *NRF2* is depends more on its translocation from the cytoplasm to the nucleus to modulate transcription of target genes, a process that does not necessarily rely on increased expression of *NRF2* (117). Alternatively, NRF2 upregulation may have occurred prior to sampling.

Oxidative stress has previously been proposed to have a role in TSD, based on the upregulation of genes involved in oxidative stress response. One of these genes, *UCP2,* was

upregulated at high male producing temperatures in *A. mississippiensis* (82). *UCP2,* and others genes involved in oxidative stress responses, were also implicated in UV induced masculinisation in larvae of a thermosensitive fish species (*Chirostoma estor*) (118). Notably, we found that *UCP2* was upregulated between stages 6 to 12 in ZZf *P. vitticeps* embryos, suggesting a sustained response to thermal stress in the mitochondria (Additional file S3).

Temperature response and cellular triage

We also observed upregulation of genes involved in response to more generalised environmental stress in ZZf compared to ZWf embryos, as expected since the embryos exposed to high temperature were experiencing a state of thermal stress (Fig. 7). Notably, *CIRBP* a promising candidate for regulation of sex determination under thermal influence, is approximately 10-fold upregulated in ZZf compared to ZWf (Additional file S3). *CIRBP* has a highly conserved role in generalised stress responses (119). It has been suggested to be a putative sex determining gene in the TSD turtle *Chelydra serpentina* (120), and is differentially expressed at different incubation temperatures in *Alligator sinensis* (81). We also observed the upregulation of *CLK4* in ZZf compared to ZWf embryos, a gene that has been recently shown to be inherently thermosensitive, and to regulate splicing of temperature specific *CIRBP* isoforms (121).

We found that *ATF5* is upregulated in ZZf embryos compared to ZWf embryos (Fig. 7). *ATF5* has diverse roles in stimulating gene expression or repression through binding of DNA regulatory elements. It is broadly involved in cell specific regulation of proliferation and differentiation, and may also be critical for activating the mitochondrial unfolded protein response (122). This gene is induced in response to various external stressors, and is activated via phosphorylation by eukaryotic translation initiation factors, two of which (*EIF1* and *EIF4A2;* Zhou et al. 2008) are also upregulated in ZZf embryos compared to ZWf embryos.

Though not well studied in the context of sex determination, heat shock factors and proteins have been implicated in female sex determination in mammals and fish, and may also play a conserved role in the ovarian pathway in *P. vitticeps* (79,124–127). Surprisingly, only one gene associated with canonical heat shock response (*HSP40,* also known as *DNAJC28*) was differentially expressed following exposure to high temperature in stage 6 ZZf

453 females compared to ZWf embryos (Additional file S3). This could mean either that a heat
454 shock response occurs prior to sampling, or that *P. vitticeps* uses different mechanisms to
455 cope with heat shock.

456 *Chromatin remodelling*

457 We observed upregulation of several components of two major chromatin remodelling
458 complexes, polycomb repressive complexes PRC1 and PRC2, in both the genotype-directed
459 ZWf and the temperature-directed ZZf female pathways in *P. vitticeps* (Fig. 7). Chromatin
460 modifier genes *KDM6B* and *JARID2* are involved in regulation of gene expression during
461 embryonic development and epigenetic modifications in response to environmental
462 stimulus (128,129). *JARID2* and *KDM6B* were both upregulated in ZZf embryos compared to
463 ZWf embryos in stages 6 and 12, and *KDM6B* was also upregulated at stage 15. These genes
464 have recently been implicated in two TSD species (*Alligator mississippiensis*, and *Trachemys*
465 *scripta*) and temperature sex reversed adult *Pogona vitticeps* (14,15,79,82).

466 We also found that two other members of the PRC1 complex, *PCGF6* and *PCGF1*, were
467 upregulated in ZZf embryos at stage 6 compared to ZWf embryos (Fig. 7). *PCGF6* is part of
468 the non-canonical PRC1 complex (ncPRC1) that mediates histone H2A mono-ubiquitination
469 at K119 (H2AK119ub) (130,131). *PCGF6* acts a master regulator for maintaining stem cell
470 identity during embryonic development (132), and is known to bind to promoters of germ
471 cell genes in developing mice (130). *PCFF1* exhibits similar functions by ensuring the proper
472 differentiation of embryonic stem cells (133). The ncPRC1 complex also promotes
473 downstream recruitment of PRC2 and H3K27me3, so that complex synergistic interactions
474 between PRC1 (both canonical and non-canonical) and PRC2 can occur (134,135).

475 We found that other components of both PRC1 and PRC2 complexes were also
476 upregulated in ZWf embryos compared to ZZf embryos (Fig. 5a, supplementary file S3). A
477 member of the canonical PRC1 complex, *PCGF2* (also known as *MEL18*), was upregulated in
478 ZWf embryos compared to ZZf embryos (134). This gene has previously been implicated in
479 temperature induced male development in *Dicentrachus labrax* (136), and is required for
480 coordinating the timing of sexual differential in female primordial germ cells in mammals
481 (137). *KDM1A*, a histone demethylase that is required for balancing cell differentiation and
482 self-renewal (138), was upregulated in ZWf embryos compared to ZZf embryos. *CHMP1A*

was upregulated in ZWf, and is likely to be involved in chromosome condensation, as well as targeting PcG proteins to regions with condensed chromatin (139).

Thus, we conclude that the initiation of sex reversal in ZZf *P. vitticeps* involves a complex cascade of cellular changes initiated by temperature. Our data are consistent with the predictions of the CaRe hypothesis that high temperatures are sensed by the cell via TRP channels, which causes an increase in intracellular increase of Ca^{2+}. Coincident with this is an increase of ROS production in the mitochondria that causes a state of oxidative stress. Together, Ca^{2+} and ROS alter the CaRe status of the cell, trigger a suite of alternations in gene expression including chromatin remodelling, which drives sex reversal (Fig. 7).

Discussion

We used the unique sex characteristics of our model reptile species, *Pogona vitticeps*, which determines sex genetically but sex reverses at high temperature, to assess predictions of the CaRe hypothesis (13). By sequencing isolated embryonic gonads, we provide the first data to represent a suite of key developmental stages with comparable tissue types, and will be a valuable resource for this reptilian model system. There are few transcriptomes of GSD reptiles during embryonic development; the only dataset available prior to this study was a preliminary study of the spiny softshell turtle, *Apalone spinifera* (126), which was inadequate for the inter-stage comparisons required to explore genetic drivers of gonad differentiation.

Our analysis of expression data during embryogenesis of normal ZWf females and temperature sex reversed ZZf females revealed for the first time differences in gene-driven and temperature-driven female development in a single species. Early in development, prior to gonad differentiation, the initiation of the sex reversal trajectory differs from the genetic female pathway both in the timing and genes involved. As development proceeds, differences in expression patterns become less until the pathways converge on a conserved developmental outcome (ovaries). Our ability to compare two female types in *P. vitticeps* allowed us to avoid previously intractable confounding factors such as sex or species-specific differences, which provided unprecedented insight into parallel female pathways. We have provided new insight to the conserved evolutionary origins of the labile networks governing environmentally sensitive sex determination pathways. We have identified a suite

of candidate genes, which now provide the necessary foundation for functional experiments in the future. This could include pharmacological manipulation of calcium signalling through alteration of intracellular calcium flux and concentration, such as interference with the TRPV4 channel, or via use of calcium chelators and ionophores, in an organ culture system (17,80). Ongoing development of resources for *P. vitticeps* as an emerging model organism may also allow for RNA interference or gene editing experiments, whereby knock-down or knock-out of candidate genes like *CIRBP*, *JARID2*, and *KDM6B*, could be used to demonstrate their roles in sex reversal (15).

The maintenance of ovarian differentiation seems to require the operation of different pathways in gene and temperature driven female development. This may involve a pathway centrally mediated by *STAT4* in sex reversed *P. vitticeps,* which has not been previously described, so requires additional confirmation with functional experiments. It will be interesting to determine if a role for these genes occurs in other species. Another STAT family gene, *STAT3*, has recently been demonstrated to play a critical role in the phosphorylation of *KDM6B* and subsequent demethylation of the *DMRT1* promoter required for male development in *T. scripta* (17). The involvement of different genes in the same family is intriguing in its implications; while different genes may be co-opted, natural selection may favour gene families with conserved functions even between evolutionarily disparate lineages.

Our data provided insight into the molecular landscape of the cell required to initiate temperature induced sex reversal. This is the first dataset to capture temperature-induced sex reversal in a reptile, and remarkably we have simultaneously implicated all functional candidates that have previously been identified to be involved in TSD across a range of other species (Table 1). Our results also identified novel genes involved with thermosensitive sex determination, and provide corroborative evidence for the CaRe hypothesis (13). Importantly, our work highlights avenues for future studies to conduct functional experiments to definitively identify the genes and pathways implicated here in sex reversal. Observation and manipulation of intracellular calcium concentrations, as has been conducted in *T. scripta* (17), will also be crucial for fully understanding the role of calcium signalling in sex reversal.

Our results highlight the complexity of initiating thermolabile systems. Indeed, it has been suggested that thermolabile sex determination involves system-wide displacement of gene regulation with multiple genes and gene products responding to temperature leading to the production of one sex or the other – a parliamentary system of sex determination (151). We take an intermediate position, arguing for a central role for Calcium-Redox balance as the proximal cellular sensor for temperature, but interacting with other required thermosensitive genes or gene products (e.g. CLK4) to influence ubiquitous signalling pathways and downstream splicing regulation, epigenetic modification and sex gene expression. The level of interaction between each thermosensitive element remains to be explored. For example, if temperature can be sensed by both *TRPV2* and *CLK4,* are both required to initiate sex reversal, or is the signal from only one sufficient? This raises the possibility that no single proximal sensor of the environmental exists, but that several thermosensitive elements early in development must come together to orchestrate alterations in gene expression.

It has been suggested that the products of TRP family genes act as mediators between the temperature signal and a cellular response through Ca^{2+} signalling and subsequent modulation of downstream gene targets (80–82). Notably, different TRP channels are implicated in two alligator species; *TRVP4* in *A. mississippiensis*, but *TRPV2, TRPC6,* and *TRPM6* in *A. sinsensis*. In *T. scripta, TRPC3* and *TRPV6* are upregulated at male producing temperatures (26°C), while *TRPM4* and *TRPV2* are upregulated at female producing temperatures (31°C), as is the case for *TRPV2* in *P. vitticeps* (79). The diversity of TRP channels recruited for roles in environmental sex determination hints at considerable evolutionary flexibility, perhaps the result of repeated and independent co-option of these channels in TSD species. As may be the case for STAT family genes, the evolution of environmentally sensitive sex determination pathways may involve the use of different genes within gene families that have conserved functions.

Our data also highlights the importance of chromatin remodelling genes in sex reversal in *P. vitticeps*. *KDM6B* and *JARID2* have been previously implicated sex differentiation in adult *P. vitticeps* (14), embryonic *T. scripta* (15,17) and embryonic *A. mississippiensis* (14). Sex-specific intron retention was observed in TSD alligators and turtle, and was exclusively associated with sex reversal in adult *P. vitticeps* (14). Subsequently,

574 knockdown of *KDM6B* in *T. scripta* caused male to female sex reversal by removing
575 methylation marks on the promoter of *DMRT1,* a gene critical in the male sex
576 determination pathway (15). *KDM6B* and *JARID2* have also been associated with TSD in
577 another turtle species (*Chrysemys picta*) (126), female to male sex change in the bluehead
578 wrasse, *Thalassoma bifasciatum* (140), and thermal responses in the European bass,
579 *Dicentrarchus labrax* (141).

580 It is currently unknown if the unique splicing events in *KDM6B* and *JARID2* in adult sex
581 reversed *P. vitticeps* that cause intron retention and presumed gene inactivation, also occur
582 in embryos. Given the high expression of these genes during embryonic development at sex
583 reversing temperatures, it would be surprising if this pattern was observed. We also show a
584 significant role for *CIRBP* as the only other gene, alongside *KDM6B*, to be consistently
585 upregulated during sex reversal in all developmental stages assessed. *CIRBP* is a mRNA
586 chaperone, which could be required to stabilise transcripts of crucial sex specific genes
587 during oxidative, cellular and/or thermal stress. It has been proposed as a novel TSD
588 candidate gene in the turtle, *Chelydra serpentina* (120). This gene remains a promising
589 candidate for mediating thermosensitive responses in TSD more broadly, and its role needs
590 to be explored in more detail.

591 ## Conclusions

592 The alternative female pathways in *P. vitticeps* demonstrates that there is inherent flexibility
593 in sex determination cascades even within the same species. This is consistent with the idea
594 that, provided a functional gonad is produced, considerable variation in sex determining and
595 differentiation processes at the early stages of development is tolerated under natural
596 selection (151). Perhaps this makes the astonishing variability in sex determination between
597 diverse species less surprising. Our findings provide novel insights, and are a critical
598 foundation for future studies of the mechanisms by which temperature determines sex.

599 ## Materials and Methods

600 *Animal breeding and egg incubations*

601 Eggs were obtained during the 2017-18 breeding season from the research breeding colony
602 at the University of Canberra. Breeding groups comprised three sex reversed females (ZZf)

603 to one male (ZZ), and three concordant females (ZWf) to two males (Fig. 1). Paternity was
604 confirmed by SNP genotyping (Fig. S2). Females were allowed to lay naturally, and eggs
605 were collected at lay or within two hours of lay. Eggs were inspected for viability as
606 indicated by presence of vasculature in the egg, and viable eggs were incubated in
607 temperature-controlled incubators (±1°C) on damp vermiculite (4 parts water to 5 parts
608 vermiculate by weight). Clutches from sex reversed females (that is, ZZf x ZZm crosses)
609 comprised eggs with only ZZ genotypes. These were initially incubated at 28°C (male
610 producing temperature, MPT) to entrain and synchronise development. After 10 d of
611 incubation, half of the eggs selected at random from each clutch was shifted to 36°C (female
612 producing temperature, FPT). Clutches from ZWf x ZZm crosses were incubated at 28°C
613 throughout the incubation period (Fig. 1A). Sample sizes are given in Fig. 1 and Additional
614 file S7.

615 *Embryo sampling and genotyping*

616 Eggs from both temperatures were sampled at times corresponding to three developmental
617 stages (6, 12 and 15) (20), taking into account the differing developmental rates between
618 28°C and 36°C. These stages equate to the bipotential gonad, recently differentiated gonad,
619 and differentiated gonad respectively (19). Embryos were euthanized by intracranial
620 injection of 0.1 ml sodium pentobarbitone (60mg/ml in isotonic saline). Individual gonads
621 were dissected from the mesonephros under a dissection microscope and snap frozen in
622 liquid nitrogen. Isolation of the gonad from the surrounding mesonephros was considered
623 essential for studying transcriptional profiles within the gonad. Embryos from three
624 different ZZf x ZZm clutches from each treatment class (temperature x stage) were selected
625 for sequencing, and randomized across sequence runs to avoid batch effects. Embryos from
626 concordant ZWf x ZZm crosses potentially yield both ZW and ZZ eggs, so these were
627 genotyped using previously established protocols (8,20). Briefly, this involved obtaining a
628 blood sample from the vasculature on the inside of the eggshell on a FTA Elute micro card
629 (Whatman). DNA was extracted from the card following the manufacturer protocols, and
630 PCR was used to amplify a W specific region (8) so allowing the identification of ZW and ZZ
631 samples.

RNA extraction and sequencing

RNA from isolated gonad samples was extracted in randomized batches using the Qiagen RNeasy Micro Kit (Cat. No. 74004) according to the manufacturer protocols. RNA was eluted in 14 µl of RNAase free water and frozen at -80°C prior to sequencing. Sequencing libraries were prepared in randomized batches using 50 ng RNA input and the Roche NimbleGen KAPA Stranded mRNA-Seq Kit (Cat. No. KK8420). Nine randomly selected samples were sequenced per lane using the Illumina HiSeq 2500 system, and 25 million read-pairs per sample were obtained on average. Read lengths of 2 x 150 bp were used. All samples were sequenced at the Kinghorn Centre for Clinical Genomics (Garvan Institute of Medical Research, Sydney). All sample RNA and library DNA was quantified using a Qubit Instrument (ThermoFisher Scientific, Scoresby, Australia), with fragment size and quality assessed using a Bioanalyzer (Agilent Technologies, Mulgrave, Australia).

Gene expression profiling

Paired-end RNA-seq libraries (.fastq format) were trimmed using trim_galore with default parameters (v0.4.1; https://www.bioinformatics.babraham.ac.uk/projects/trim_galore/, last access 21-Apr-2020). Trimmed reads were aligned to the *Pogona vitticeps* NCBI reference genome (pvi1.1, GenBank GCA_900067755.1; (142)) using STAR (v2.5.3; (143)), with splice-aware alignment guided by the accompanying NCBI gene (*Pvi1.1*) annotation (.gtf format). Likely PCR duplicates and non-unique alignments were removed using samtools (v1.5 ; (144)). Gene expression counts and normalised expression values (reported in TPM) were determined using RSEM (rsem-calculate-expression; v1.3.1; (145)).

Identification of non-sex reversed specimens

Normalised transcripts per million (TPM) for a panel of sex-specific genes (*SOX9, AMH, DMRT1, FOXL2, CYP19A1, CYP17A1*) were inspected across the three stages to identify if any samples showed aberrant expression patterns. This approach was also used to determine if any of the stage 12 and 15 samples from the 36°C treatment had not undergone sex reversal by comparing expression levels between ZWf and ZZf embryos; the rate of sex reversal is 96% at 36°C (8) (Fig. S3, Additional file S8). The five samples from clutch 9 exhibited significantly higher expression values for *SOX9, AMH*, and *DMRT1* and represented clear outliers. This was also supported by multidimensional scaling (MDS) plots, so the

decision was made to regard the five samples from clutch 9 as aberrant and exclude them from subsequent analyses (Figs S3, S4, Additional file S9). Any ZZf samples with male-like gene expression patterns (high expression for male-specific genes, and low expression for female-specific genes) were considered to have not been reversed (sex reversal is not 100% at 36°C) and were removed (two stage 15 samples).

Differential expression analysis

Differential expression analysis of ZZf and ZWf transcripts was conducted on raw counts using the EdgeR package (Bioconductor v 3.9 (146)) in R (v 1.2.1335, (147)), following standard procedures outlined in the EdgeR users guide (146,148). Lowly expressed genes, which was applied to genes with fewer than ten counts across three samples, were removed from the raw counts (19,285 genes) so that the total number of genes retained was 17,075. Following conversion to a DGElist object in EdgeR, raw counts were normalised using the upper-quartile method (calcNormFactors function) (149). Estimates for common negative binomial dispersion parameters were generated (estimateGLMCommonDisp function) (148), followed by generation of empirical Bayes dispersion estimates for each gene (estimateGLMTagwiseDisp function) (148,150). A quasi-likelihood binomial generalised log-linear model was fitted (glmQLFit function) and the glmQFTest function was used to compare contrasts within the design matrix (151–155). A P-value cut-off of 0.01 and a $\log_2$-fold change threshold of 1 or -1 was applied to all contrasts (topTags function) (151). Contrasts were used to assess differential expression between ZZf and ZWf samples across each developmental stage. Raw count (Additional file S10) and expression files (Additional file S11) from this analysis are supplied.

Gene ontology (GO) analysis was conducted for each set of differentially expressed genes using GOrilla (156,157). The filtered count data file (17,075 genes) was used for the background gene set at a P-value threshold of 10^{-3}.

K-means clustering analysis

K-means clustering analysis was performed on normalised counts per million extracted from the DGElist object produced by the initial process of the DGE analysis using edgeR (see above). Counts for each gene were averaged for each treatment group, and the number of clusters was selected using the sum of squared error approach, which was further validated

by checking that each cluster centroid was poorly correlated with all other cluster centroids (maximum correlation 0.703 in ZWf clusters, and 0.65 in ZZf clusters). A total of 6 clusters was chosen, and clustering analysis was conducted using the kmeans function in R package stats v3.6.2. Resultant gene lists were sorted by unique and shared genes between clusters with similar trends between ZWf and ZZf (cluster 1 in ZWf, cluster 3 in ZZf, and cluster 3 in ZWf and cluster 5 in ZZf). Both unique and shared genes from each cluster and pairs of clusters (cluster 1 and 3, and clusters 3 and 5) were then analysed for gene ontology (GO) enrichment using GOrilla (156,157). The filtered count data file (17,075 genes) was used for the background gene set at a P-value threshold of 10^{-3}.

Declarations

Ethics Approval

All procedures were conducted in accordance with approved animal ethics protocols from the University of Canberra Animal Ethics Committee (AEC 17-17).

Consent for publication

Not applicable

Availability of data and materials

The raw input files (counts and transcripts per million) that were analysed for this study are available as supplementary files. Raw sequencing data is available under NCBI BioProject PRJNA699086 (Biosample accession IDs SAMN17765903 to SAMN17765941).

Competing interests

The authors declare that they have no competing interests.

Funding

This work was supported by a Discovery Grant from the Australian Research Council (DP170101147) awarded to AG (lead), CEH, JD, JMG, Tariq Ezaz, Stephen Sarre, Lisa Schwanz and Paul Waters. SLW was supported by a CSIRO Research Plus Postgraduate Award and a Research Training Scholarship.

Author Contributions

AG and CEH led and designed the experiment, AG and JMG built the "Sex in Dragons" program of which this is a part. SLW carried out all experimental procedures and differential gene expression analysis. JB created all RNA libraries and carried out all sequencing. IWD generated all data files from sequencing outputs. SW assisted with data analysis, particularly K-means clustering. SLW lead the preparation of the manuscript, with AG, CEH, and JMG. All authors provided feedback on the manuscript and approved the final draft.

Acknowledgements

We thank Dr Wendy Ruscoe and Jacqui Richardson at the University of Canberra Animal House Facility for their animal husbandry expertise.

References

1. Koopman P, Gubbay J, Vivian N, Goodfellow P, Lovell-Badge R. Male development of chromosomally female mice transgenic for *Sry*. Nature. 1991;351:117–21.

2. Sinclair AH, Berta P, Palmer MS, Hawkins JR, Griffiths BL, Smith MJ, et al. A gene from the human sex-determining region encodes a protein with homology to a conserved DNA-binding motif. Nature. 1990;346:240–4.

3. Smith CA, Roeszler KN, Ohnesorg T, Cummins DM, Farlie PG, Doran TJ, et al. The avian Z-linked gene DMRT1 is required for male sex determination in the chicken. Nature. 2009;461:267–71.

4. Barske LA, Capel B. Blurring the edges in vertebrate sex determination. Curr Opin Genet Dev. 2008;18:499–505

5. Capel B. Vertebrate sex determination: evolutionary plasticity of a fundamental switch. Nat Rev Genet. 2017;18:675–89.

6. Sarre SD, Georges A, Quinn A. The ends of a continuum: Genetic and temperature-dependent sex determination in reptiles. BioEssays. 2004;26:639–45.

7. Holleley CE, Sarre SD, O'Meally D, Georges A. Sex reversal in reptiles: Reproductive oddity or powerful driver of evolutionary change? Sex Dev. 2016;10:279–87.

8. Holleley CE, O'Meally D, Sarre SD, Graves J, Ezaz T, Matsubara K, et al. Sex reversal triggers the rapid transition from genetic to temperature-dependent sex. Nature. 2015;523:79–82.

9. Radder RS, Quinn AE, Georges A, Sarre SD, Shine R, Quinn AE, et al. Genetic evidence for co-occurrence of chromosomal and thermal sex-determining systems in a lizard. Biol Lett. 2008;4:176–8.

10. Bachtrog D, Mank JE, Peichel CL, Kirkpatrick M, Otto SP, Ashman T-L, et al. Sex Determination: Why So Many Ways of Doing It? PLOS Biol. 2014;12:e1001899.

751 11. Herpin A, Schartl M. Plasticity of gene-regulatory networks controlling sex determination: Of
752 masters, slaves, usual suspects, newcomers, and usurpators. EMBO Rep. 2015;16:1260–74.

753 12. Singh SK, Das D, Rhen T. Embryonic temperature programs phenotype in reptiles. Front
754 Physiol. 2020; doi: 10.3389/fphys.2020.00035.

755 13. Castelli M, Whiteley S, Georges A, Holleley C. Cellular calcium and redox regulation: The
756 mediator of vertebrate environmental sex determination? Biol Rev. 2020;95:680–95.

757 14. Deveson IW, Holleley CE, Blackburn J, Marshall Graves JA, Mattick JS, Waters PD, et al.
758 Differential intron retention in Jumonji chromatin modifier genes is implicated in reptile
759 temperature-dependent sex determination. Sci Adv. 2017;3:e1700731.

760 15. Ge C, Ye J, Weber C, Sun W, Zhang H, Zhou Y, et al. The histone demethylase KDM6B
761 regulates temperature-dependent sex determination in a turtle species. Science. 2018;360:645–8.

762 16. Georges A, Holleley CE. How does temperature determine sex? Science. 2018;360:601–2.

763 17. Weber C, Zhou Y, Lee J, Looger L, Qian G, Ge C, et al. Temperature-dependent sex
764 determination is mediated by pSTAT3 repression of *Kdm6b*. Science. 2020;3:303–6.

765 18. Quinn AE, Georges A, Sarre SD, Guarino F, Ezaz T, Graves JAM. Temperature sex reversal
766 implies sex gene dosage in a reptile. Science. 2007;316:411.

767 19. Whiteley SL, Weisbecker V, Georges A, Gauthier ARG, Whitehead DL, Holleley CE.
768 Developmental asynchrony and antagonism of sex determination pathways in a lizard with
769 temperature-induced sex reversal. Sci Rep. 2018;8:1–9.

770 20. Whiteley SL, Holleley CE, Ruscoe WA, Castelli M, Whitehead DL, Lei J, et al. Sex
771 determination mode does not affect body or genital development of the central bearded dragon
772 (*Pogona vitticeps*). Evodevo. 2017; doi.org/10.1186.

773 21. Ross A, Munger S, Capel B. *Bmp7* regulates germ cell proliferation in mouse fetal gonads. Sex
774 Dev. 2007;1:127–37.

775 22. Windley SP, Wilhelm D. Signaling pathways involved in mammalian sex determination and
776 gonad development. Sex Dev. 2016;9:297–315.

777 23. Tang H, Brennan J, Karl J, Hamada Y, Raetzman L, Capel B. Notch signaling maintains Leydig
778 progenitor cells in the mouse testis. Development. 2008;135:3745–53.

779 24. Krone N, Hanley NA, Arlt W. Age-specific changes in sex steroid biosynthesis and sex
780 development. Best Pract Res Clin Endocrinol Metab. 2007;21:393–401.

781 25. Russell DW, Wilson JD. Steroid 5a-Rreducatse□: Two genes/two enzymes. Annu Rev
782 Biochem. 1994;63:25–61.

783 26. Eid W, Opitz L, Biason-Lauber A. Genome-wide identification of CBX2 targets: Insights in the
784 human sex development network. Mol Endocrinol. 2015;29:247–57.

785 27. Gnessi L, Basciani S, Mariani S, Arizzi M, Spera G, Wang C, et al. Leydig cell loss and
786 spermatogenic arrest in platelet-derived growth factor (PDGF)-A-deficient mice. J Cell Biol.
787 2000;149:1019–25.

788 28. Schmahl J, Rizzolo K, Soriano P. The PDGF signaling pathway controls multiple steroid-
789 producing lineages. Genes Dev. 2008;22:3255–67.

790 29. Chawengsaksophak K, Svingen T, Ng ET, Epp T, Spiller CM, Clark C, et al. Loss of *Wnt5a*
791 disrupts primordial germ cell migration and male sexual development in mice. Biol Reprod.
792 2011;86:1–12.

793 30. Warr N, Siggers P, Bogani D, Brixey R, Pastorelli L, Yates L, et al. *Sfrp1* and *Sfrp2* are required
794 for normal male sexual development in mice. Dev Biol. 2009;326:273–84.

795 31. Kollara A, Brown TJ. Variable expression of nuclear receptor coactivator 4 (*NcoA4*) during
796 mouse embryonic development. J Histochem Cytochem. 2010;58:595–609.

797 32. Padua MB, Jiang T, Morse DA, Fox SC, Hatch HM, Tevosian SG. Combined loss of the *GATA4*
798 and *GATA6* transcription factors in male mice disrupts testicular development and confers adrenal-
799 like function in the testes. Endocrinology. 2015;156:1873–86.

800 33. Sarraj M, Chua HK, Umbers A, Loveland K, Findlay J, Stenvers KL. Differential expression of
801 *TGFBR3* (betaglycan) in mouse ovary and testis during gonadogenesis. Growth Factors. 2007;25:334–
802 45.

803 34. Carré GA, Couty I, Hennequet-Antier C, Govoroun MS. Gene expression profiling reveals new
804 potential players of gonad differentiation in the chicken embryo. PLoS One. 2011;6:1–12.

805 35. Zhao L, Arsenault M, Ng ET, Longmuss E, Chau TCY, Hartwig S, et al. *SOX4* regulates gonad
806 morphogenesis and promotes male germ cell differentiation in mice. Dev Biol. 2017;423:46–56.

807 36. Adolfi MC, Nakajima RT, N RH, Schartl M. Intersex, hermaphroditism, and gonadal plasticity
808 in vertebrates: Evolution of the Mullerian duct and *Amh/Amhr2* signaling. Annu Rev Anim Biosci.
809 2019;7:149–72.

810 37. Sekido R, Lovell-Badge R. Sex determination involves synergistic action of SRY and SF1 on a
811 specific *Sox9* enhancer. Nature. 2008;453:930–4.

812 38. Rhen T, Schroeder A. Molecular mechanisms of sex determination in reptiles. Sex Dev.
813 2010;4:16–28.

814 39. Simon AR, Rai U, Fanburg BL, Cochran BH. Activation of the JAK-STAT pathway by reactive
815 oxygen species. Am J Physiol Physiol. 1998;275:C1640–52.

816 40. Good SR, Thieu VT, Mathur AN, Yu Q, Stritesky GL, Yeh N, et al. Temporal induction pattern
817 of STAT4 target genes defines potential for Th1 lineage-specific programming. J Immunol.
818 2009;183:3839–47.

819 41. Rawlings JS, Rosler KM, Harrison DA. The JAK/STAT signaling pathway. J Cell Sci.
820 2004;117:1281–3.

821 42. Eggers S, Ohnesorg T, Sinclair A. Genetic regulation of mammalian gonad development. Nat
822 Rev Endocrinol. 2014;10:673–83.

823 43. Wang DS, Kobayashi T, Zhou LY, Paul-Prasanth B, Ijiri S, Sakai F, et al. *Foxl2* up-regulates
824 aromatase gene transcription in a female-specific manner by binding to the promoter as well as
825 interacting with *Ad4* binding protein/steroidogenic factor. Mol Endocrinol. 2007;21:712–25.

826 44. Park M, Shin E, Won M, Kim JH, Go H, Kim HL, et al. *FOXL2* interacts with steroidogenic
827 factor-1 (*SF-1*) and represses SF-1-induced *CYP17* transcription in granulosa cells. Mol Endocrinol.
828 2010;24:1024–36.

829 45. Lei N, Heckert LL. *Sp1* and *Egr1* Regulate Transcription of the *Dmrt1* Gene in Sertoli Cells. Biol
830 Reprod. 2002;66:675–84.

831 46. Topilko P, Schneider-Maunoury S, Levi G, Trembleau A, Gourdji D, Driancourt MA, et al.
832 Multiple pituitary and ovarian defects in *Krox-24* (*NGFI-A*, *Egr-1*)- targeted mice. Mol Endocrinol.
833 1998;12:107–22.

834 47. Lee SL, Sadovsky Y, Swirnoff AH, Polish JA. Luteinizing hormone deficiency and female
835 infertility in mice lacking. Science. 1996;273:1219-21.

836 48. Cutting A, Chue J, Smith CA. Just how conserved is vertebrate sex determination? Dev Dyn.
837 2013;242:380–7.

838 49. Lydon JP, DeMayo FJ, Funk CR, Mani SK, Hughes AR, Montgomery CA, et al. Mice lacking
839 progesterone receptor exhibit pleiotropic reproductive abnormalities. Genes Dev. 1995;9:2266–78.

840 50. Birk OS, Casiano DE, Wassif CA, Cogliati T, Zhao L, Zhao Y, et al. The LIM homeobox gene
841 *Lhx9* is essential for mouse gonad formation. Nature. 2000;403:909–13.

842 51. Oréal E, Mazaud S, Picard JY, Magre S, Carré-Eusébe D. Different patterns of anti-Müllerian
843 hormone expression, as related to *DMRT1, SF-1, WT1, GATA-4, Wnt-4*, and *Lhx9* expression, in the
844 chick differentiating gonads. Dev Dyn. 2002;225:221–32.

845 52. Wilhelm D, Englert C. The Wilms tumor suppressor *WT1* regulates early gonad development
846 by activation of *Sf1*. Genes Dev. 2002;16:1839–51.

847 53. Duester G. Families of retinoid dehydrogenases regulating vitamin A function: Production of
848 visual pigment and retinoic acid. Eur J Biochem. 2000;267:4315–24.

849 54. Bowles J, Knight D, Smith C, Wilhelm D, Richman J, Mamiya S, et al. Retinoid signaling
850 determines germ cell fate in mice. Science. 2006;312:596–9.

851 55. Koubova J, Menke DB, Zhou Q, Cape B, Griswold MD, Page DC. Retinoic acid regulates sex-
852 specific timing of meiotic initiation in mice. Proc Natl Acad Sci. 2006;103:2474–9.

853 56. Roes J, Choi BK, Power D, Xu P, Segal AW. Granulocyte function in grancalcin-deficient mice.
854 Mol Cell Biol. 2003;23:826–30.

855 57. Maki M, Kitaura Y, Satoh H, Ohkouchi S, Shibata H. Structures, functions and molecular
856 evolution of the penta-EF-hand Ca^{2+}-binding proteins. Biochim Biophys Acta - Proteins Proteomics.
857 2002;1600(1–2):51–60.

858 58. Lloyd S. Least squares quantization in PCM. IEEE Trans Inf Theory. 1982;28:129–37.

859 59. Nef S, Schaad O, Stallings NR, Cederroth CR, Pitetti JL, Schaer G, et al. Gene expression
860 during sex determination reveals a robust female genetic program at the onset of ovarian
861 development. Dev Biol. 2005;287:361–77.

862 60. Greenlee AR, Shiao MS, Snyder E, Buaas FW, Gu T, Stearns TM, et al. Deregulated sex
863 chromosome gene expression with male germ cell-specific loss of *Dicer1*. PLoS One. 2012;7:1–13.

61. Koenig PA, Nicholls PK, Schmidt FI, Hagiwara M, Maruyama T, Frydman GH, et al. The E2 ubiquitin-conjugating enzyme *UBE2J1* is required for spermiogenesis in mice. J Biol Chem. 2014;289:34490–502.

62. La Fortezza M, Schenk M, Cosolo A, Kolybaba A, Grass I, Classen AK. JAK/STAT signalling mediates cell survival in response to tissue stress. Dev. 2016;143:2907–19.

63. Paul A, Wilson S, Belham CM, Robinson CJM, Scott PH, Gould GW, et al. Stress-activated protein kinases: Activation, regulation and function. Cell Signal. 1997;9:403–10.

64. Davis RJ. Signal transduction by the JNK group of MAP kinases. Cell. 2000;103:239–52.

65. Wang X, Martindale JL, Liu Y, Holbrook NJ. The cellular response to oxidative stress: influences of mitogen-activated protein kinase signalling pathways on cell survival. Biochem J. 1998;333:291–300.

66. Martinez P, Thanasoula M, Carlos AR, Gómez-López G, Tejera AM, Schoeftner S, et al. Mammalian *Rap1* controls telomere function and gene expression through binding to telomeric and extratelomeric sites. Nat Cell Biol. 2010;12:768–80.

67. Teo H, Ghosh S, Luesch H, Ghosh A, Wong ET, Malik N, et al. Telomere-independent *Rap1* is an IKK adaptor and regulates NF-κB-dependent gene expression. Nat Cell Biol. 2010;12:758–67.

68. Gilmore TD. Introduction to NF-κB: players, pathways, perspectives. Oncogene. 2006;25:6680.

69. Morgan MJ, Liu Z. Crosstalk of reactive oxygen species and NF-κB signaling. Cell Res. 2011;21:103–15.

70. Oeckinghaus A, Hayden MS, Ghosh S. Crosstalk in NF-κB signaling pathways. Nat Immunol. 2011;12:695–708.

71. McGuire NL, Bentley GE. Neuropeptides in the gonads: From evolution to pharmacology. Front Pharmacol. 2010;1:1–13.

72. Ulrich-Lai YM, Herman JP. Neural regulation of endocrine and autonomic stress responses. Nat Rev Neurosci. 2009;10:397–409.

73. Todd E V, Liu H, Muncaster S, Gemmell NJ. Bending genders: The biology of natural sex change in fish. Sex Dev. 2016 Mar;10:223–41.

74. Liu J, Liu X, Jin C, Du X, He Y, Zhang Q. Transcriptome profiling insights the feature of sex reversal induced by high temperature in tongue sole *Cynoglossus semilaevis*. Front Genet. 2019;10:1-15.

75. Wang Q, Liu K, Feng B, Zhang Z, Wang R, Tang L, et al. Gonad transcriptome analysis of high temperature induced sex reversal in Chinese Tongue Sole, *Cynoglossus semilaevis*. Front Genet. 2019;10:1-11.

76. Hattori R, Castaneda-Cortes D, Arias Padilla L, Strobl-Mazzulla P, Fernandino J. Activation of stress response axis as a key process in environment induced sex plasticity in fish. Cell Mol Life Sci. 2020; doi.org/10(0123456789).

77. Hilton JK, Rath P, Helsell CVM, Beckstein O, Van Horn WD. Understanding thermosensitive transient receptor potential channels as versatile polymodal cellular sensors. Biochemistry. 2015;54:2401–13.

78. Benham CD, Gunthorpe MJ, Davis JB. TRPV channels as temperature sensors. Cell Calcium. 2003;33:479–87.

79. Czerwinski M, Natarajan A, Barske L, Looger LL, Capel B. A timecourse analysis of systemic and gonadal effects of temperature on sexual development of the red-eared slider turtle *Trachemys scripta elegans*. Dev Biol. 2016;420:166–77.

80. Yatsu R, Miyagawa S, Kohno S, Saito S, Lowers RH, Ogino Y, et al. *TRPV4* associates environmental temperature and sex determination in the American alligator. Sci Rep. 2015;5:1–10.

81. Lin JQ, Zhou Q, Yang HQ, Fang LM, Tang KY, Sun L, et al. Molecular mechanism of temperature-dependent sex determination and differentiation in Chinese alligator revealed by developmental transcriptome profiling. Sci Bull. 2018;63:209–12.

82. Yatsu R, Miyagawa S, Kohno S, Parrott BB, Yamaguchi K, Ogino Y, et al. RNA-seq analysis of the gonadal transcriptome during *Alligator mississippiensis* temperature-dependent sex determination and differentiation. BMC Genomics. 2016;77:1-13.

83. Maynard Case R, Eisner D, Gurney A, Jones O, Muallem S, Verkhratsky A. Evolution of calcium homeostasis: From birth of the first cell to an omnipresent signalling system. Cell Calcium. 2007;42:345–50.

84. Carafoli E. The calcium-signalling saga: Tap water and protein crystals. Nat Rev Mol Cell Biol. 2003;4:326–32.

85. Penna E, Espino J, De Stefani D, Rizzuto R. The MCU complex in cell death. Cell Calcium. 2018;69:73–80.

86. Hoffman NE, Zhang X, Gill DL, Shanmughapriya S, Rajan S, Jog NR, et al. Ca^{2+} signals regulate mitochondrial metabolism by stimulating CREB-mediated expression of the mitochondrial Ca^{2+} uniporter gene MCU. Sci Signal. 2015;8:73-80.

87. Strehler E, Caride A, Filoteo A, Xiong Y, Penniston J, Enyedi A. Plasma membrane Ca^{2+}-ATPases as dynamic regulators of cellular calcium handling. Ann N Y Acad Sci. 2013; doi:10.1196.

88. Stocker M. Ca^{2+}-activated K^{+} channels: Molecular determinants and function of the SK family. Nat Rev Neurosci. 2004;5:758–70.

89. Faber ESL, Sah P. Functions of SK channels in central neurons. Clin Exp Pharmacol Physiol. 2007;34:1077–83.

90. Catterall W. Structure and regulation of voltage-gated Ca^{2+} channels. Annu Rev Immunol. 2004;22:485–501.

91. Campiglio M, Flucher BE. The role of auxiliary subunits for the functional diversity of voltage-gated calcium channels. J Cell Physiol. 2015;230:2019–31.

92. Kumar A, Kumari S, Majhi RK, Swain N, Yadav M, Goswami C. Regulation of TRP channels by steroids: Implications in physiology and diseases. Gen Comp Endocrinol. 2015;220:23–32.

939 93. Miehe S, Crause P, Schmidt T, Löhn M, Kleemann HW, Licher T, et al. Inhibition of
940 diacylglycerol-sensitive TRPC channels by synthetic and natural steroids. PLoS One. 2012;7:e35393.

941 94. Ramsey IS, Delling M, Clapham DE. An introduction to TRP channels. Annu Rev Physiol.
942 2006;68:619–47.

943 95. Schaefer M, Plant TD, Obukhov AG, Hofmann T, Gudermann T, Schultz G. Receptor-mediated
944 regulation of the nonselective cation channels TRPC4 and TRPC5. J Biol Chem. 2000;275:17517–26.

945 96. Brostrom MA, Brostrom CO. Calcium dynamics and endoplasmic reticular function in the
946 regulation of protein synthesis: Implications for cell growth and adaptability. Cell Calcium.
947 2003;34:345–63.

948 97. Michalak M, Corbett EF, Mesaeli N, Nakamura K, Opas M. Calreticulin: One protein, one
949 gene, many functions. Biochem J. 1999;344:281–92.

950 98. Dedhar S. Novel functions for calreticulin: interaction with integrins and modulation of gene
951 expression? Trends Biochem Sci. 1994;19:269–71.

952 99. Echevarria W, Leite MF, Guerra MT, Zipfel WR, Nathanson MH. Regulation of calcium signals
953 in the nucleus by a nucleoplasmic reticulum. Nat Cell Biol. 2003;5:440–6.

954 100. Burns K, Duggan B, Atkinson EA, Famulski KS, Nemer M, Bleackley RC, et al. Modulation of
955 gene expression by calreticulin binding to the glucocorticoid receptor. Nature. 1994;367:476–80.

956 101. Michalak M, Burns K, Andrin C, Mesaeli N, Jass GH, Busaan JL, et al. Endoplasmic reticulum
957 form of calreticulin modulates glucocorticoid- sensitive gene expression. J Biol Chem.
958 1996;271:29436–45.

959 102. Wang X, Su M, Gao F, Xie W, Zeng Y, Li D, et al. Structural basis for activity of TRIC counter-
960 ion channels in calcium release. Proc Natl Acad Sci. 2019;116:4238–43.

961 103. Santamaria-Kisiel L, Rintala-Dempsey A, Shaw G. Calcium-dependent and -independent
962 interactions of the S100 protein family. Biochem J. 2006;396:201–14.

963 104. Heizmann C. S-100 proteins. In: Offermanns S, Rosenthal W, editors. Encyclopedia of
964 Molecular Pharmacology. Berlin: Springer; 2008. p. 123–45.

965 105. Heizmann CW. S100 proteins: structure, functions and pathology. Front Biosci.
966 2002;7:d1356.

967 106. Rebecchi MJ, Pentyala SN. Structure, function, and control of phosphoinositide-specific
968 phospholipase C. Physiol Rev. 2000;80:1291–335.

969 107. Thannickal V, Fanburg B. Reactive oxygen species in cell signaling. Am J Physiol - Lung Cell
970 Mol Physiol. 2000;279:1005–28.

971 108. Temple MD, Perrone GG, Dawes IW. Complex cellular responses to reactive oxygen species.
972 Trends Cell Biol. 2005;15:319–26.

973 109. Schenk H, Klein M, Erdbrügger W, Dröge W, Schulze-Osthoff K. Distinct effects of thioredoxin
974 and antioxidants on the activation of transcription factors NF-kappa B and AP-1. Proc Natl Acad Sci.
975 1994;91:1672–6.

976 110. Matsuzawa A. Thioredoxin and redox signaling: Roles of the thioredoxin system in control of
977 cell fate. Arch Biochem Biophys. 2017;617:101–5.

978 111. Van Der Vos KE, Coffer PJ. FOXO-binding partners: It takes two to tango. Oncogene.
979 2008;27:2289–99.

980 112. Tao GZ, Lehwald N, Jang KY, Baek J, Xu B, Omary MB, et al. Wnt/β-catenin signaling protects
981 mouse liver against oxidative stress-induced apoptosis through the inhibition of forkhead
982 transcription factor *FoxO3*. J Biol Chem. 2013;288:17214–24.

983 113. Xiong Y, Uys JD, Tew KD, Townsend DM. S-Glutathionylation: From molecular mechanisms to
984 health outcomes. Antioxid Redox Signal. 2011;15:233–70.

985 114. Yankovskaya V, Horsefield R, Törnroth S, Luna-Chavez C, Miyoshi H, Léger C, et al.
986 Architecture of succinate dehydrogenase and reactive oxygen species generation. Science.
987 2003;299:700–4.

988 115. Mikhed Y, Görlach A, Knaus UG, Daiber A. Redox regulation of genome stability by effects on
989 gene expression, epigenetic pathways and DNA damage/repair. Redox Biol. 2015;5:275–89.

990 116. Cho SS, Kim KM, Yang JH, Kim JY, Park SJ, Kim SJ, et al. Induction of *REDD1* via *AP-1* prevents
991 oxidative stress-mediated injury in hepatocytes. Free Radic Biol Med [Internet]. 2018;124:221–31.
992 Available from: https://doi.org/10.1016/j.freeradbiomed.2018.06.014

993 117. Tonelli C, Chio I, Tuveson D. Transcriptional Regulation by *Nrf2*. Antioxidants Redox Signal.
994 2018;29:1727–45.

995 118. Corona-Herrera GA, Arranz SE, Martínez-Palacios CA, Navarrete-Ramírez P, Toledo-Cuevas
996 EM, Valdez-Alarcón JJ, et al. Experimental evidence of masculinization by continuous illumination in
997 a temperature sex determination teleost (Atherinopsidae) model: is oxidative stress involved? J Fish
998 Biol. 2018;93:229–37.

999 119. Zhong P, Huang H. Recent progress in the research of cold-inducible RNA-binding protein.
1000 Future Sci OA. 2017;3:FSO246.

1001 120. Schroeder AL, Metzger KJ, Miller A, Rhen T. A novel candidate gene for temperature-
1002 dependent sex determination in the Common Snapping Turtle. Genetics. 2016;203:557–71.

1003 121. Haltenhof T, Kotte A, de Bortoli F, Schiefer S, Meinke S, Emmerichs A-K, et al. A conserved
1004 kinase-based body temperature sensor globally controls alternative splicing and gene expression.
1005 Mol Cell. 2020;78:1–13.

1006 122. Wang YT, Lim Y, McCall MN, Huang K-T, Haynes CM, Nehrke K, et al. Cardioprotection by the
1007 mitochondrial unfolded protein response requires ATF5. Am J Physiol Circ Physiol. 2019;317:H472–8.

1008 123. Zhou D, Palam LR, Jiang L, Narasimhan J, Staschke KA, Wek RC. Phosphorylation of *eIF2*
1009 directs *ATF5* translational control in response to diverse stress conditions. J Biol Chem.
1010 2008;283:7064–73.

1011 124. Furukawa F, Hamasaki S, Hara S, Uchimura T, Shiraishi E, Osafune N, et al. Heat shock factor
1012 1 protects germ cell proliferation during early ovarian differentiation in medaka. Sci Rep.
1013 2019;6927:1-10.

1014 125. Metchat A, Akerfelt M, Bierkamp C, Delsinne V, Sistonen L, Alexandre H, et al. Mammalian
1015 heat shock factor 1 is essential for oocyte meiosis and directly regulates *Hsp90α* expression. J Biol
1016 Chem. 2009;284:9521–8.

1017 126. Radhakrishnan S, Literman R, Neuwald J, Severin A, Valenzuela N. Transcriptomic responses
1018 to environmental temperature by turtles with temperature-dependent and genotypic sex
1019 determination assessed by RNAseq inform the genetic architecture of embryonic gonadal
1020 development. PLoS One. 2017;12:e0172044.

1021 127. Kohno S, Katsu Y, Urushitani H, Ohta Y, Iguchi T, Guillette JLJ. Potential contributions of heat
1022 shock proteins to temperature-dependent sex determination in the American Alligator. Sex Dev.
1023 2010;4:73–87.

1024 128. Aloia L, Di Stefano B, Di Croce L. Polycomb complexes in stem cells and embryonic
1025 development. Development. 2013;140:2525–34.

1026 129. Marasca F, Bodega B, Orlando V. How polycomb-mediated cell memory deals with a
1027 changing environment: Variations in PcG complexes and proteins assortment convey plasticity to
1028 epigenetic regulation as a response to environment. Bioessays. 2018;40:1–13.

1029 130. Endoh M, Endo TA, Shinga J, Hayashi K, Farcas A, Ma KW, et al. PCGF6-PRC1 suppresses
1030 premature differentiation of mouse embryonic stem cells by regulating germ cell-related genes.
1031 Elife. 2017;6:1–26.

1032 131. Cohen I, Bar C, Ezhkova E. Activity of PRC1 and histone H2AK119 monoubiquitination⍰:
1033 Revising popular misconceptions. Bioessays. 2020;1900192:1–8.

1034 132. Yang CS, Chang KY, Dang J, Rana TM. Polycomb group protein *Pcgf6* acts as a master
1035 regulator to maintain embryonic stem cell identity. Sci Rep. 2016;6:1–12.

1036 133. Yan Y, Zhao W, Huang Y, Tong H, Xia Y, Jiang Q, et al. Loss of polycomb group protein *Pcgf1*
1037 severely compromises proper differentiation of embryonic stem cells. Sci Rep. 2017;7:1–11.

1038 134. Fursova NA, Blackledge NP, Nakayama M, Ito S, Koseki Y, Farcas AM, et al. Synergy between
1039 variant PRC1 complexes defines polycomb-mediated gene repression. Mol Cell. 2019;74:1020-36

1040 135. Blackledge NP, Farcas AM, Kondo T, King HW, McGouran JF, Hanssen LLP, et al. Variant PRC1
1041 complex-dependent H2A ubiquitylation drives PRC2 recruitment and polycomb domain formation.
1042 Cell. 2014;157:1445–59.

1043 136. Díaz N, Piferrer F. Lasting effects of early exposure to temperature on the gonadal
1044 transcriptome at the time of sex differentiation in the European sea bass, a fish with mixed genetic
1045 and environmental sex determination. BMC Genomics. 2015 Dec;16:2–16.

1046 137. Yokobayashi S, Liang CY, Kohler H, Nestorov P, Liu Z, Vidal M, et al. PRC1 coordinates timing
1047 of sexual differentiation of female primordial germ cells. Nature. 2013;495:236–40.

1048 138. Shen H, Xu W, Lan F. Histone lysine demethylases in mammalian embryonic development.
1049 Exp Mol Med. 2017;49:e325-7.

1050 139. Stauffer DR, Howard TL, Nyun T, Hollenberg SM. *CHMP1* is a novel nuclear matrix protein
1051 affecting chromatin structure and cell-cycle progression. J Cell Sci. 2001;114:2383–93.

1052 140. Todd E V, Ortega-Recalde O, Liu H, Lamm MS, Rutherford KM, Cross H, et al. Stress, novel sex
1053 genes and epigenetic reprogramming orchestrate socially-controlled sex change. Sci Adv.
1054 2019;5:eaaw7006.

1055 141. Ribas L, Crespo B, Xavier D, Kuhl H, Rodríguez JM, Díaz N, et al. Characterization of the
1056 European Sea Bass (*Dicentrarchus labrax*) gonadal transcriptome during sexual development. Mar
1057 Biotechnol. 2019;21:359–73.

1058 142. Georges A, Li Q, Lian J, O'Meally D, Deakin J, Wang Z, et al. High-coverage sequencing and
1059 annotated assembly of the genome of the Australian dragon lizard *Pogona vitticeps*. Gigascience.
1060 2015;45:1-10.

1061 143. Dobin A, Davis CA, Schlesinger F, Drenkow J, Zaleski C, Jha S, et al. STAR: Ultrafast universal
1062 RNA-seq aligner. Bioinformatics. 2013;29:15–21.

1063 144. Li H, Handsaker B, Wysoker A, Fennell T, Ruan J, Homer N, et al. The Sequence
1064 Alignment/Map format and SAMtools. Bioinformatics. 2009;25:2078–9.

1065 145. Li B, Dewey CN. RSEM: accurate transcript quantification from RNA-Seq data with or without
1066 a reference genome. BMC Bioinformatics. 2011;12:21–40.

1067 146. Robinson MD, McCarthy DJ, Smyth GK. edgeR: A Bioconductor package for differential
1068 expression analysis of digital gene expression data. Bioinformatics. 2009;26:139–40.

1069 147. RStudio: Integrated development for R. Boston: RStudio Inc; 2015.

1070 148. McCarthy DJ, Chen Y, Smyth GK. Differential expression analysis of multifactor RNA-Seq
1071 experiments with respect to biological variation. Nucleic Acids Res. 2012;40:4288–97.

1072 149. Anders S, Huber W. Differential expression analysis for sequence count data. Genome Biol.
1073 2010;11:R106.

1074 150. Cox DR, Reid N. Parameter orthogonality and approximate conditional inference. J R Stat Soc
1075 B. 1987;49:1–39.

1076 151. Chen Y, Lun ATL, Smyth GK. From reads to genes to pathways: Differential expression
1077 analysis of RNA-Seq experiments using Rsubread and the edgeR quasi-likelihood pipeline.
1078 F1000Research. 2016;5:1–49.

1079 152. Lun A, Chen Y, Smyth G. It's DE-licious: A recipe for differential expression analyses of RNA-
1080 seq experiments using quasi-likelihood methods in edgeR. In: Mathe E, Davis S, editors. Statistical
1081 Genomics. New York: Humana Press; 2016. p. 391–416.

1082 153. Lund SP, Nettleton D, McCarthy DJ, Smyth GK. Detecting differential expression in RNA-
1083 sequence data using quasi-likelihood with shrunken dispersion estimates. Stat Appl Genet Mol Biol.
1084 2012;11:1-42.

1085 154. Lun ATL, Smyth GK. No counts, no variance: allowing for loss of degrees of freedom when
1086 assessing biological variability from RNA-seq data. Stat Appl Genet Mol Biol. 2017;16:83–93.

1087 155. Phipson B, Lee S, Majewski IJ, Alexander WS, Smyth GK. Robust hyperparameter estimation
1088 protects against hypervariable genes and improves power to detect differential expression. Ann Appl
1089 Stat. 2016;10:946–63.

1090 156. Eden E, Navon R, Steinfeld I, Lipson D, Yakhini Z. GOrilla: a tool for discovery and
1091 visualization of enriched GO terms in ranked gene lists. BMC Bioinformatics. 2009;10:48.

1092 157. Eden E, Lipson D, Yogev S, Yakhini Z. Discovering motifs in ranked lists of DNA sequences.
1093 PLoS Comput Biol. 2007;3:0508–22.

1094

1095 **Table 1**: All genes, full gene names, functional categories and associations with either gene
1096 (ZWf) or temperature driven (ZZf) female development mentioned in the paper. NA denotes
1097 a gene that was mentioned, but was not differentially expressed. Genes with an asterisk are
1098 those that have previously been implicated in thermosensitive sex determination cascades,
1099 either in *Pogona vitticeps*, or in another reptile species.

Gene ID	Gene Name	Functional Category	Association
ADAD1	Adenosine deaminase domain containing 1 [testis-specific]	Sex determination and differentiation (Male-specific)	ZWf/ZZf
ALDH1A2	Retinal dehydrogenase 2	Sex determination and differentiation (Male-specific)	ZWf
AMH	Anti-Müllerian hormone	Sex determination and differentiation	NA
AMHR2	Anti-Müllerian hormone receptor 2	Sex determination and differentiation	ZZf
ATF5	Activating transcription factor 5	Stress response	ZZf
ATP2B1	ATPase plasma membrane Ca^{2+} transporting 1	Calcium signalling	ZZf
ATP2B4	ATPase plasma membrane Ca^{2+} transporting 4	Calcium signalling	ZZf
BMP7	Bone morphogenetic protein 7	Sex determination and differentiation	ZZf
C2CD2	C2 calcium-dependent domain containing 2	Calcium signalling	ZZf
C2CD2L	C2 calcium-dependent domain containing 2 like	Calcium signalling	ZZf
CACNB3	Calcium voltage-gated channel auxiliary subunit beta 3	Calcium signalling	ZZf
CALM1	Calmodulin 1	Calcium signalling	ZWf/ZZf
CALR	Calreticulin	Calcium signalling	ZZf
CAMKK1	Calcium/calmodulin dependent protein kinase kinase 1	Calcium signalling	ZZf
CHMP1A	Chromatin modifying protein 1A	Chromatin remodelling	ZWf
CIRBP*	Cold-inducible binding protein	Temperature-sensing	ZZf
CLK4*	CDC like kinase 4	Temperature-sensing	ZZf
CRH	Corticotropin releasing hormone/factor	Stress response	ZWf
CYP17A1	Cytochrome P450 17A1	Sex determination and differentiation (Female-Specific)	ZWf/ZZf
CYP19A1	Aromatase	Sex determination and differentiation (Female-	ZWf/ZZf

		Specific)	
DDIT4	DNA damage inducible transcript 4	DNA damage repair	ZZf
DLL3	Delta like canonical Notch ligand 3	Sex determination and differentiation (Male-specific)	ZWf/ZZf
DLL4	Delta like canonical Notch ligand 4	Sex determination and differentiation (Male-specific)	ZWf/ZZf
DMRT1	Doublesex and mab-3 related transcription factor 1	Sex determination and differentiation (Male-specific)	NA
EGR1	Early growth response 1	Sex determination and differentiation	ZZf
EIF1	Eukaryotic translation initiation factor 1	Translation initiation	ZZf
EIF4A2	Eukaryotic translation initiation factor 4A2	Translation initiation	ZZf
ENDOD1	Endonuclease domain containing 1	DNA damage repair	ZZf
ESR2	Estrogen receptor 2	Sex determination and differentiation (Female-Specific)	ZWf
ESRRG	Estrogen related receptor gamma	Sex determination and differentiation (Female-Specific)	ZZf
FIGLA	Folliculogeneisis specific basic helix-loop-helix	Sex determination and differentiation (Female-Specific)	ZWf/ZZf
FOXL2	Forkhead box L2	Sex determination and differentiation (Female-Specific)	ZWf/ZZf
FOXO3	Forkhead box O3	Redox regulation	ZZf
FZD1	Frizzled class receptor 1	Sex determination and differentiation	ZZf
GADD45G	Growth arrest and DNA damage inducible gamma	Sex determination and differentiation	ZWf
GATA6	GATA binding factor 6	Sex determination and differentiation	ZWf
GCA	Grancalcin	Calcium signalling	ZWf
GLRX	Glutaredoxin	Redox regulation	ZZf
GPX1	Glutathione peroxidase	Redox regulation	ZZf
HERC2	HECT and RLD domain containing E3 ubiquitin protein ligase 2	DNA damage repair	ZZf
HNRNPUL1	Heterogeneous nuclear ribonucleoprotein U like 1	Splicing	ZWf/ZZf
HSD17B3	Hydroxysteroid 17-beta dehydrogenase 3	Sex determination and differentiation	ZZf
HSP40	DnaJ heat shock protein family (hsp40) member B1	Temperature-sensing	ZZf
HSP90AB1	Heat shock protein 90 alpha family class B member 1	Temperature-sensing	ZWf/ZZf
HSPA4	Heat shock protein family A (Hsp70) member 4	Temperature-sensing	ZWf/ZZf
HSPB1	Heat shock protein family B (Small) member 1	Temperature-sensing	ZWf/ZZf

HSPB11	Heat shock protein family B (Small) member 11	Temperature-sensing	ZWf/ZZf
HSPD1	Heat shock protein family D (Hsp60) member 1	Temperature-sensing	ZWf/ZZf
HSPH1	Heat shock protein family H (Hsp110) member 1	Temperature-sensing	ZWf/ZZf
IKBKG/NEMO	NF-κB essential modulator	NF-kB pathway	ZWf
JAG2	Jagged 2	Sex determination and differentiation	ZWf
JARID2*	Jumonji and AT-rich interaction domain containing 2	Chromatin remodelling	ZZf
KCNN1	Small conductance calcium-activated potassium channel protein 1	Calcium signalling	ZZf
KCTD1	Potassium channel tetramerization domain containing 1	Sex determination and differentiation (Male-specific)	ZZf
KDM1A	Lysine demethylase 1A	Chromatin remodelling	ZWf/ZZf
KDM2B	Lysine demethylase 2B	Chromatin remodelling	ZWf/ZZf
KDM3B	Lysine demethylase 3B	Chromatin remodelling	ZWf/ZZf
KDM5B	Lysine demethylase 5B	Chromatin remodelling	ZWf/ZZf
KDM6B*	Lysine demethylase 6B	Chromatin remodelling	ZZf
LHX9	LIM homeobox 9	DNA damage repair	ZWf
LIG4	DNA ligase 4	DNA damage repair	ZZf
MAP3K8	Mitogen-activated protein kinase kinase kinase 8	Stress response	ZWf/ZZf
MAPK1	Mitogen-activated protein kinase 1	Stress response	ZWf/ZZf
MAPK9	Mitogen-activated protein kinase 9	Stress response	ZWf/ZZf
MCU	Mitochondrial calcium uniporter	Calcium signalling	ZZf
MGST1	Microsomal glutathione S-transferase 1	Redox regulation	ZZf
NANOS1	Nanos C2HC-type zinc finger 1	Sex determination and differentiation (Female-Specific)	ZWf
NCOA4	Nuclear receptor coactivator 4	Sex determination and differentiation	ZZf
NEIL3	Nei like DNA glycosylase 3	DNA damage repair	ZZf
NR5A1	Nuclear receptor subfamily 5 group A member 1	Sex determination and differentiation	ZZf
NRF2	Nuclear factor, erythroid 2 like 2	Redox regulation	NA
PCGF1	Polycomb group ring finger 1	Chromatin remodelling	ZZf
PCGF2/Mel18	Polycomb group ring finger 2	Chromatin remodelling	ZWf
PCGF6	Polycomb group ring finger 6	Chromatin remodelling	ZZf
PCYOX1L	Prenylcysteine oxidate 1 like	Redox regulation	ZZf

PDGFB	Platelet derived growth factor subunit B, paralog of mammalian *PDGFA*	Sex determination and differentiation	ZZf
PGR	Progesterone receptor	Sex determination and differentiation (Female-Specific)	ZWf
PLCB1	Phospholipase C Beta 1	Calcium signalling	ZZf
PLCL2	Phospholipase C like 2	Calcium signalling	ZZf
POMC	Proopiomelanocortin	Stress response	NA
PRDX3	Peroiredoxin 3	Redox regulation	ZZf
PRKCI	Protein kinase C iota	NF-kB pathway	ZWf
RSPO1	R-spondin 1	Sex determination and differentiation (Female-Specific)	ZWf/ZZf
S100Z	S100 calcium binding protein Z	Calcium signalling	ZZf
SFRP2	Secreted frizzled related protein 2	Sex determination and differentiation (Male-specific)	ZZf
SOX4	SRY-box transcription factor 4	Sex determination and differentiation (Male-specific)	ZWf
SOX9	Sry-box 9	Sex determination and differentiation (Male-specific)	NA
SQOR	Sulfide quinone oxidoreductase	Redox regulation	ZZf
SRD5A2	Steroid 5 alpha reductase 2	Sex determination and differentiation	ZWf
STAT1	Signal transducer and activator of transcription 1	Stress response	ZWf
STAT4	Signal transducer and activator of transcription 4	Stress response	ZZf
STRA8	Stimulated by retinoic acid 8	Sex determination and differentiation	ZWf/ZZf
TERF2IP	Telomeric repeat-binding factor 2-interacting protein 1	NF-kB pathway	ZWf
TGFBR3L	Transforming growth factor beta receptor 3-like, paralog of mammalian *TGFBR3*	Sex determination and differentiation	ZZf
TMEM38B/TRICB	Trimeric intracellular cation channel type B	Calcium signalling	ZZf
TRPC4	Transient receptor potential cation channel subfamily C member 4	Temperature-sensing	ZZf
TRPV2*	Transient receptor potential cation channel subfamily V member 2	Temperature-sensing	ZZf
TXNDC11	Thioredoxin domain containing 11	Redox regulation	ZZf
UBE2J1	Ubiquitin-conjugating enzyme E2 J1	Sex determination and differentiation	ZWf/ZZf
UCP2	Oxidative stress responsive-gene uncoupling protein-2	Redox regulation	ZZf
WNT5a	Wnt family member 5a	Sex determination and differentiation	ZZf

1100

Figure Captions

Fig. 1: Schematic representation of experimental design used in this study to compare the differences between genetic sex determination and temperature dependent sex determination. (**A**) Summary of experiment showing how the parental crosses were designed, and how eggs were allocated and incubated. Eggs from sex reversed females (ZZf) were initially incubated at 28°C for 10 days, then were switched to 36°C. Eggs were sampled at the same three developmental stages (6, 12, and 15) based on (19,20). At stage 6 the gonad is bipotential, at stage 12 the gonad is in the early stages of differentiation, and it completely differentiated by stage 15. Eggs from concordant females (ZWf) were incubated at 28°C and sampled at the same three developmental stages as the ZZf eggs. (**B**) PCA plots showing the first and second principal components of read count per gene between ZZf (red) and ZWf (blue) at each stage of development.

Fig. 2: Schematic overview of gene-driven (blue) and temperature-driven (red) female developmental pathways in *Pogona vitticeps*. The pathways are initially different (from stages 6 to 12), but they ultimately converge on highly similar expression profiles when ovarian differentiation has occurred by stage 15. Both pathways are characterised by repression of a male signal, however this signal is stronger in temperature-driven females and appears to require ongoing repression when compared with the gene-driven females.

Fig. 3: (**A**) Expression (transcripts per million, TPM) ± SE of three genes differentially expressed at all three developmental stages between ZZf and ZWf, with *KDM6B* and *CIRPB* (outlined in red) having consistently higher expression in ZZf embryos, and *GCA* having higher expression in ZWf. (**B**) Bar graphs representing the number of differentially expressed genes in all comparisons between ZZf and ZWf, and between developmental stages. MA plots of this data are available in Fig. S1. Differentially expressed genes were determined as having *P* values ≤ 0.01 and $\log_2$-fold changes of 1, -1.

Fig. 4: Hypothesized pathway for the maintenance of the ovarian phenotype in stage 12 sex reversed ZZf *Pogona vitticeps*. Given the upregulation of these genes, it is likely that reactive oxygen species induce the phosphorylation, and subsequent activation and nuclear translocation of STAT4, likely mediated by PDGFB. Once in the nucleus, STAT4 is able to bind

1130 to promoter regions of known target genes, *NR5A1, AMHR2* and *EGR2* to regulate their
1131 expression and promote ovarian development.

1132 **Fig. 5**: (**A**) A subset of GO processes and (**C**) GO functions enriched in stage 6 ZZf embryos
1133 compared with ZWf. (**B**) A subset of GO processes and (**D**) GO functions enriched in stage 6
1134 ZWf embryos compared with ZZf. Complete results of GO analysis for all developmental
1135 stages in ZZf and ZWf for enriched GO processes and functions is provided in Additional file
1136 S2. Differentially expressed chromatin modifier (**E**) and cellular stress (**F**) genes in *Pogona*
1137 *vitticeps* at stage 6 comparing ZWf and ZZf females.

1138 **Fig. 6**: K-means clustering analysis on normalized counts per million for ZZf (**A**) and ZWf (**B**)
1139 across all developmental stages. The colour depicts the correlation score of each gene in the
1140 cluster, where numbers approaching one (red) have the strongest correlation. All gene lists
1141 produced for each cluster are provided in Additional file S5.

1142 **Fig. 7**: Hypothesised cellular environment (*A*) of a ZZf gonad at stage 6 in *Pogona vitticeps*
1143 based on differential expression analysis (*B*) using the CaRe model as a framework (13). We
1144 used this approach to understand the cellular context responsible for driving sex reversal in
1145 ZZf samples. This reveals that calcium signalling likely plays a very important role in
1146 mediating the temperature signal to determine sex. Influx of intracellular calcium is likely
1147 mediated primarily by TRPV2, and may also be influenced by KCNN1 and CACNB3. This influx
1148 appears to trigger significant changes in the cell to maintain calcium homeostasis. MCU,
1149 ATP2B1, CALR and TRICB all play a role in this process by sequestering calcium and pumping
1150 it back out of the cell, in which KCNN1 and CACNB3 may have a role. Calcium signalling
1151 molecules C2CD2, C2CDL2, and S100Z are likely responsible for encoding and translating the
1152 calcium signal leading to changes in gene transcription. Changes in gene expression are
1153 likely mediated primarily by the two major Polycomb Repressive Complexes, PRC1 and
1154 PRC2. Members of these two complexes (PCGF1, PCGF6, KDM6B, and JARID2)
1155 transcriptionally regulate genes by controlling methylation dynamics of their targets, the
1156 latter two of which have been previously implicated in sex reversal (14,15). ATF5 may also
1157 play a role in gene regulation, and alternative splicing, which has been implicated in sex
1158 reversal (14) may be mediated by CLK4. High temperatures necessarily increase cellular
1159 metabolism, which in turn increases the amount of reactive oxygen species (ROS) produced
1160 by the mitochondria. ROS can cause cellular damage at high levels, so trigger an antioxidant

response, which is observed here in the upregulation of MGST1, PRDX3, TXNDC11 and FOXO3. Also of note is the upregulation of CIRBP, which has numerous functions in response to diverse cellular stresses, and has been implicated in TSD.

Supplementary Materials

Additional file S1: Differentially expressed genes between developmental stages 6 and 12, and 12 and 15 for ZZf and ZWf females generated from EdgeR's "topTags" function. Results are sorted by log-fold change, with a cut-off of 1 or -1 applied, and a P-value threshold of 0.01. For the stage 6 and 12 comparison, genes with positive log-fold changes are upregulated at stage 12, while for the stage 12 and 15 comparison, genes with a positive log-fold change are upregulated at stage 15. No genes were differentially expressed between stages 12 and 15 in ZZf females.

Additional file S2: Gene ontology (GO) enrichment for process and function for the stage 6 and 12 comparison for ZZf and ZWf (Additional file S1). GO enrichment was not possible for the stage 12 and 15 comparison because differentially expressed genes were lacking. GO enrichment was generated from GOrilla (156,157) at a significance threshold of $P \leq 0.05$.

Additional file S3: Differentially expressed genes between ZZf and ZWf for each developmental stage generated from EdgeR's "topTags" function. Results are sorted by log-fold change, with a cut-off of 1 or -1 applied, and a P-value threshold of 0.01 Genes with positive log-fold changes are upregulated in ZZf embryos, genes with negative log-fold changes are upregulated in ZWf.

Additional file S4: Gene ontology (GO) enrichment for process and function generated from GOrilla (156,157) at a significance threshold of $P \leq 0.05$ for differentially expressed genes at stages 6 and 12 for ZZf and ZWf samples (Additional file S3).

Additional file S5: Gene list outputs for K-means clustering analysis (n = 6), and comparative information for matched clusters between ZZf and ZWf (ZZC1 and ZWC1, and ZZC2 and ZWC4) including genes that are unique and shared between each cluster.

Additional file S6: Gene ontology (GO) process and function enrichment for genes in ZZf C1, and genes shared between ZZC5 and ZWC3 generated from GOrilla (156,157) at a significance threshold of $P \leq 0.05$.

Additional file S7: Summary of all embryonic gonad samples sequenced for this study, including incubation temperature, genotype, parental cross, developmental stage, and clutch for each sample. Unique sample identifiers are matched to those used in raw data inputs (Additional file S10, S11).

Additional file S8: Outputs from pairwise T-tests conducted between stage 15 (n = 7) and stage 15 ZZf samples suspected not to have undergone sex reversal (n = 2). The normalised transcripts per million (TPM) for six genes, three male (*AMH, DMRT1, SOX9*) and three female genes (*FOXL2, CYP19A1, CYP17A1*) were used. The two samples suspected of not undergoing sex reversal show significantly different expression levels for four of these genes, and differences just above the significance threshold of ≤0.05 for the other two genes. On this basis, these two samples were removed from further analysis.

Additional file S9: Outputs from one way analysis of variance (ANOVAs) between all clutches (clutch 1, 2, 3, 6, and 9) across each developmental stage (6, 12 and 15) for a panel of sex specific genes (*AMH, SOX9* and *DMRT1*) to determine whether clutch 9 exhibits aberrant expression levels. The normalised transcripts per million (TPM) generates from the EdgeR pipeline described in the materials and methods was used. Based on the results from this analysis, five samples from clutch 9 were excluded from further analysis.

Additional file S10: Raw counts for all samples (n = 39) for all genes (n = 19,284) prior to any filtering or sample removal. Sample ID labels correspond to incubation temperature (36 or 28), maternal genotype/maternal homozygosity/maternal heterozygosity (ZZf or ZWf), sample stage (s1 = stage 6, s2 = stage 12, s3 = stage 15), clutch number (c1, c2, etc.), and replicate ID (e.g., "a" denotes the sample was the first replicate for that sampling point). Sample data is also available in Additional file S7.

Additional file S11: Raw expression values (TPM, transcripts per million) all samples (n = 39) for all genes (n = 19,284) prior to any filtering or sample removal. Sample ID labels correspond to incubation temperature (36 or 28), maternal genotype/maternal

homozygosity/maternal heterozygosity (ZZf or ZWf), sample stage (s1 = stage 6, s2 = stage 12, s3 = stage 15), clutch number (c1, c2, etc.), and replicate ID (e.g., "a" denotes the sample was the first replicate for that sampling point). Sample data is also available in Additional file S7.

Fig. S1: MA plots of read counts per gene from differential expression analysis conducted between ZZf and ZWf (**A**) and comparisons between stages for both ZZf and ZW (**B**). Differentially expressed genes (*P* values ≤ 0.01, $\log_2$-fold change of 1, -1) are coloured (colour indicative of significant fold change), and the total number of genes are indicated in each plot. Grey indicates no differential expression, horizontal lines indicate $\log_2$-fold changes of 1, -1. CPM: normalised counts per million

Fig. S2: Network analysis of parental and offspring SNPs to confirm paternity of clutches used in this experiment. SNP data was generated by Dart sequencing, a reduced genome representation sequencing method at Diversity Arrays Technology, University of Canberra.

Fig. S3: Expression (TPM, transcripts per million) of female-specific genes (*CYP17A1, FOXL2, CYP19A1*; panel A) and male-specific genes (*DMRT1, SOX9, AMH*; panel B) across three developmental stages (6, 12, 15) (19,20) for all samples to aid in the identification of samples with aberrant expression patterns. Samples from later developmental stages that exhibit low expression of female-specific genes are likely to have not undergone sex reversal. Sample ID labels correspond to incubation temperature (36°C or 28°C in red or blue respectively), maternal genotype/maternal homozygosity/maternal heterozygosity (ZZf or ZWf), sample stage (s1 = stage 6, s2 = stage 12, s3 = stage 15), clutch number (c1, c2, etc.), and replicate ID (e.g., "a" denotes the sample was the first replicate for that sampling point).

Fig. S4: Principal components analysis (PCA) plots performed on normalised counts per million for filtered genes following the EdgeR pipeline described in the materials and methods section. (*A*) PCA of all samples (n = 39) (*B*) PCA of samples with clutch 9 removed (n = 32) (*C*) PCA of samples with clutch 9 samples removed and two samples that had not undergone sex reversal. This is the final dataset upon which all analysis was performed (n = 30).

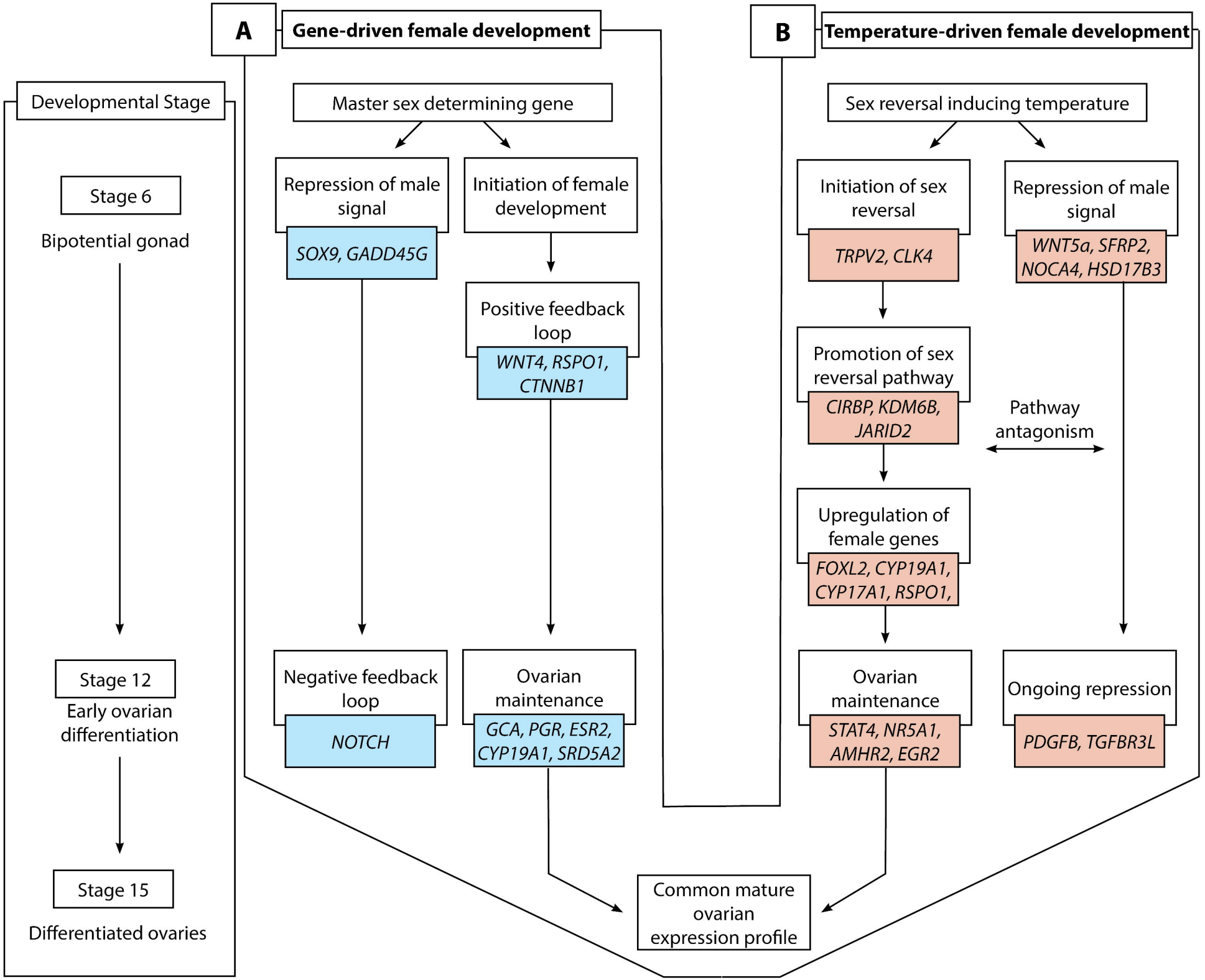
A
Gene-driven female development
B
Temperature-driven female development
Developmental Stage
Stage 6
Bipotential gonad
Stage 12
Early ovarian differentiation
Stage 15
Differentiated ovaries
Master sex determining gene
Repression of male signal
SOX9, GADD45G
Initiation of female development
Positive feedback loop
WNT4, RSPO1, CTNNB1
Negative feedback loop
NOTCH
Ovarian maintenance
GCA, PGR, ESR2, CYP19A1, SRD5A2
Sex reversal inducing temperature
Initiation of sex reversal
TRPV2, CLK4
Repression of male signal
WNT5a, SFRP2, NOCA4, HSD17B3
Promotion of sex reversal pathway
CIRBP, KDM6B, JARID2
Pathway antagonism
Upregulation of female genes
FOXL2, CYP19A1, CYP17A1, RSPO1,
Ovarian maintenance
STAT4, NR5A1, AMHR2, EGR2
Ongoing repression
PDGFB, TGFBR3L
Common mature ovarian expression profile

A

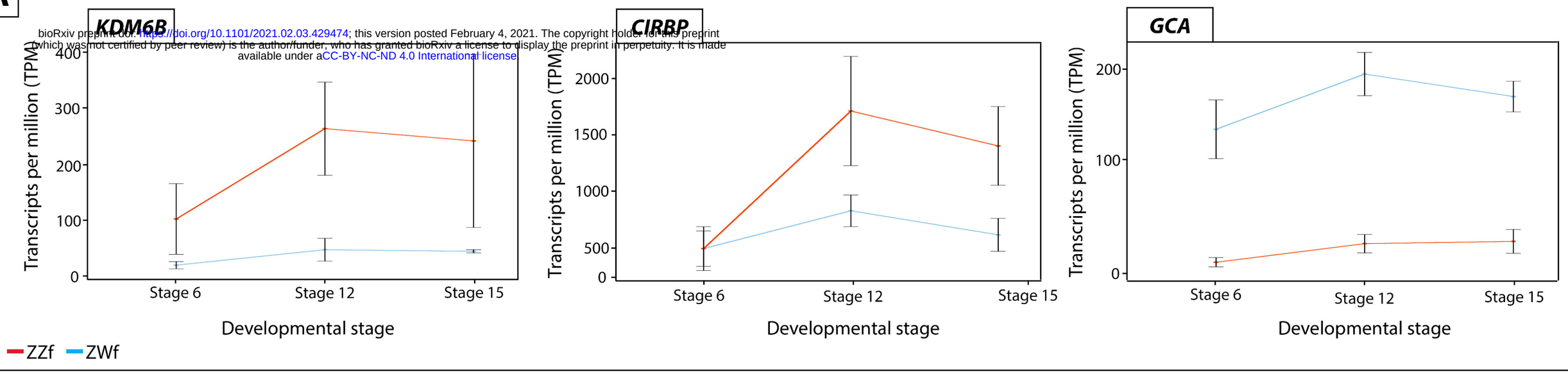

B

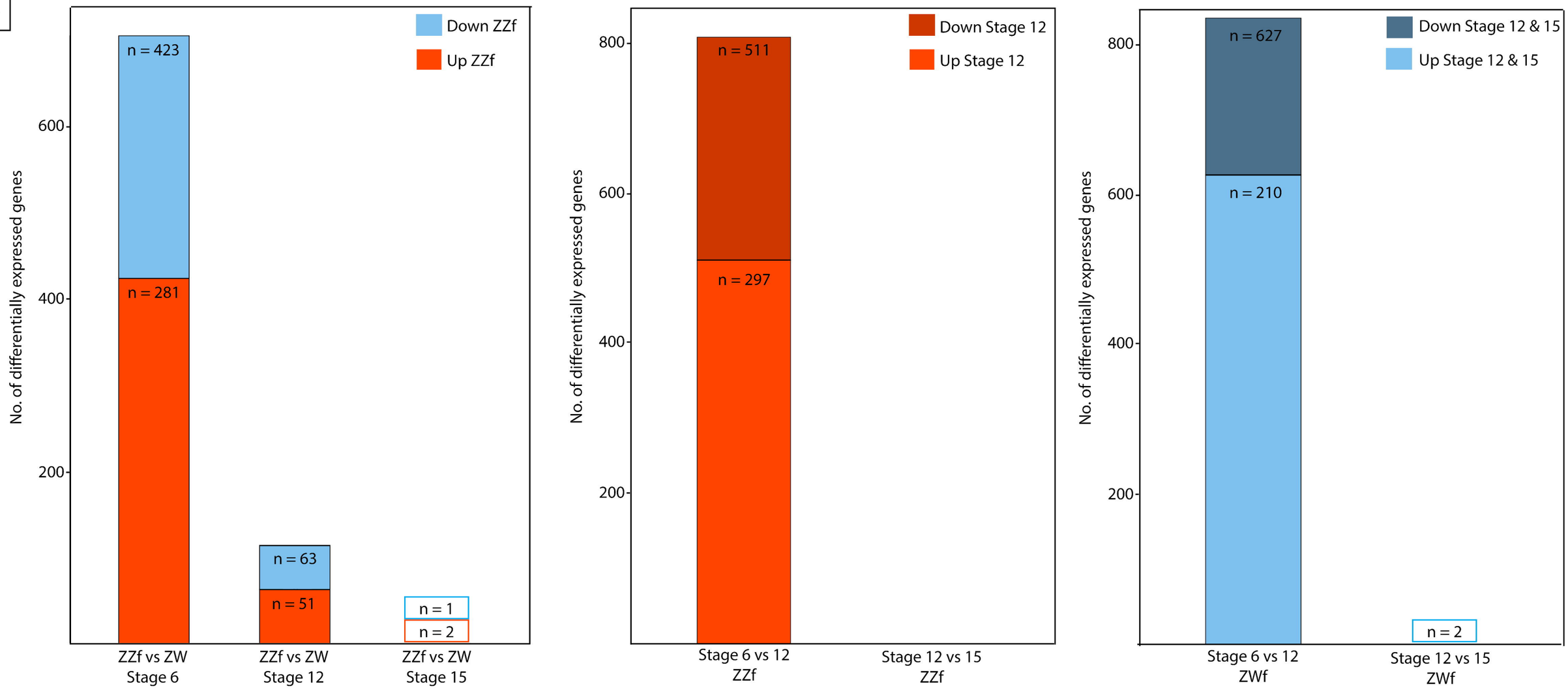

A

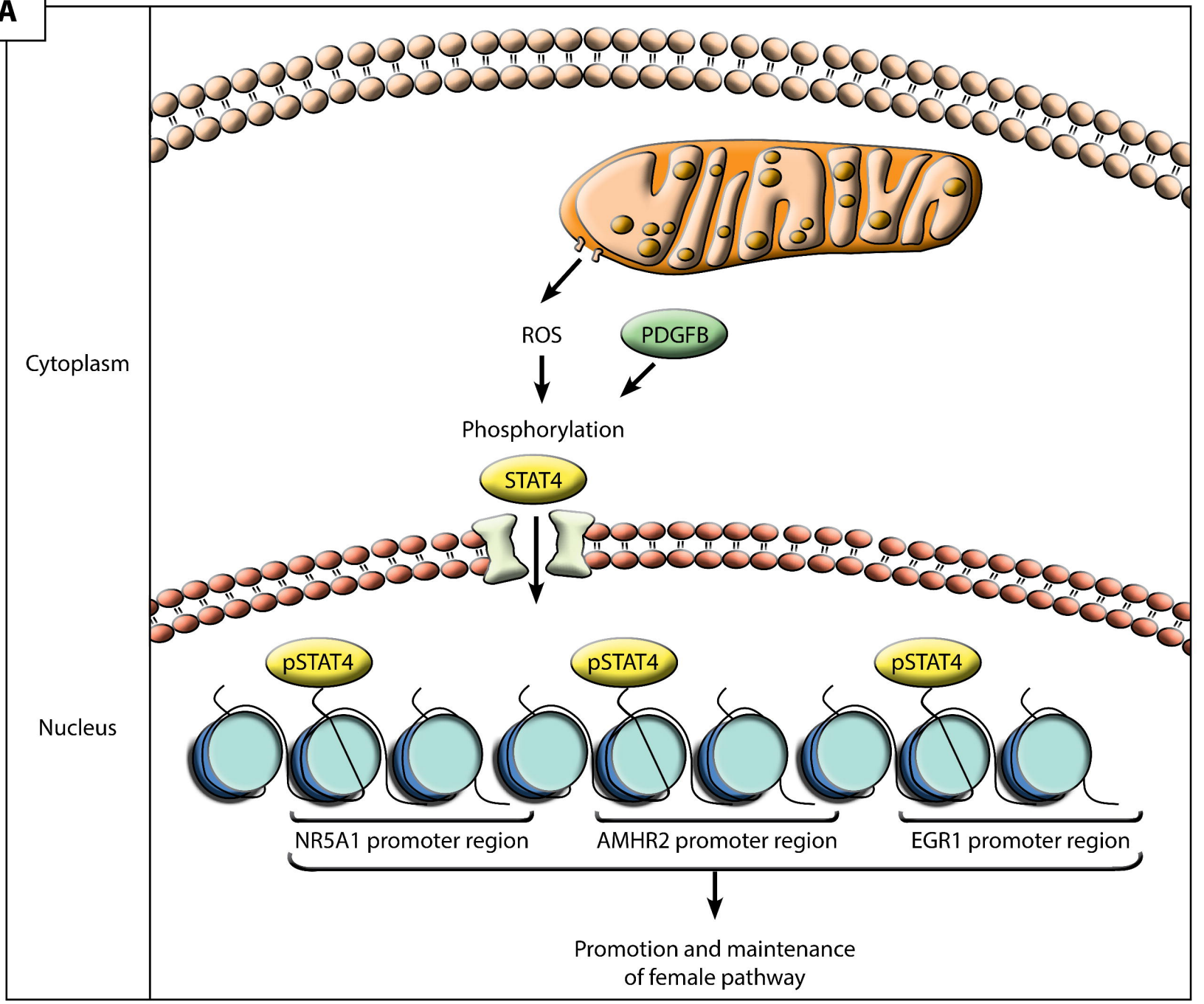

B

Gene ID	Gene Name	Log FC	Log CPM	F	P-value	FDR
AMHR2	Anti-Müllerian hormone receptor type 2	-1.96	7.85	23.49	3.17E-5	1.56E-3
EGR1	Early growth response 1	-2.58	5.74	30.80	4.14E-6	4.05E-4
NR5A1	Nuclear receptor subfamily 5 group A member 1	-1.30	7.87	15.21	4.69E-4	9.66E-3
PDGFB	Platelet derived growth factor subunit B	-2.83	4.58	72.33	1.10E-9	2.35E-6
STAT4	Signal transducer and activator of transcription 4	-1.36	3.57	16.94	2.56E-4	6.47E-3

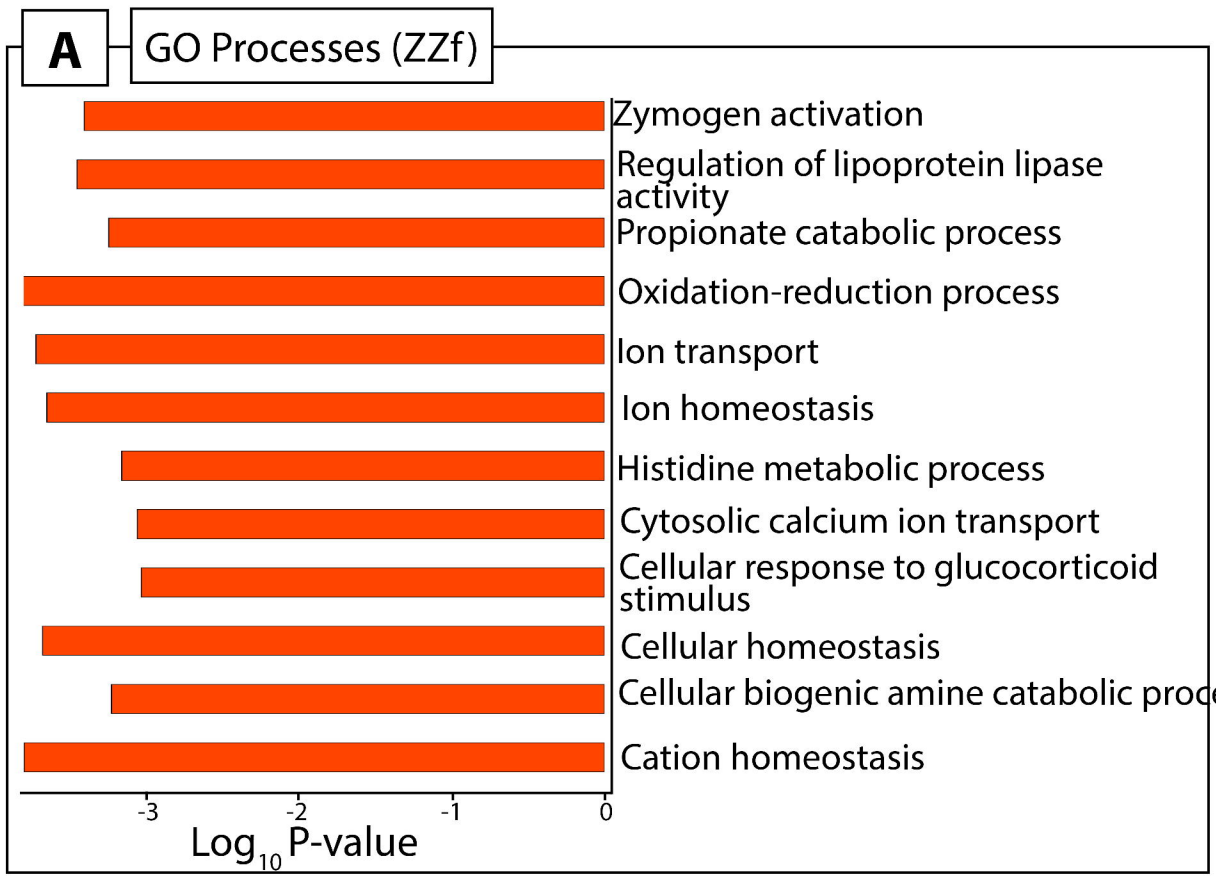

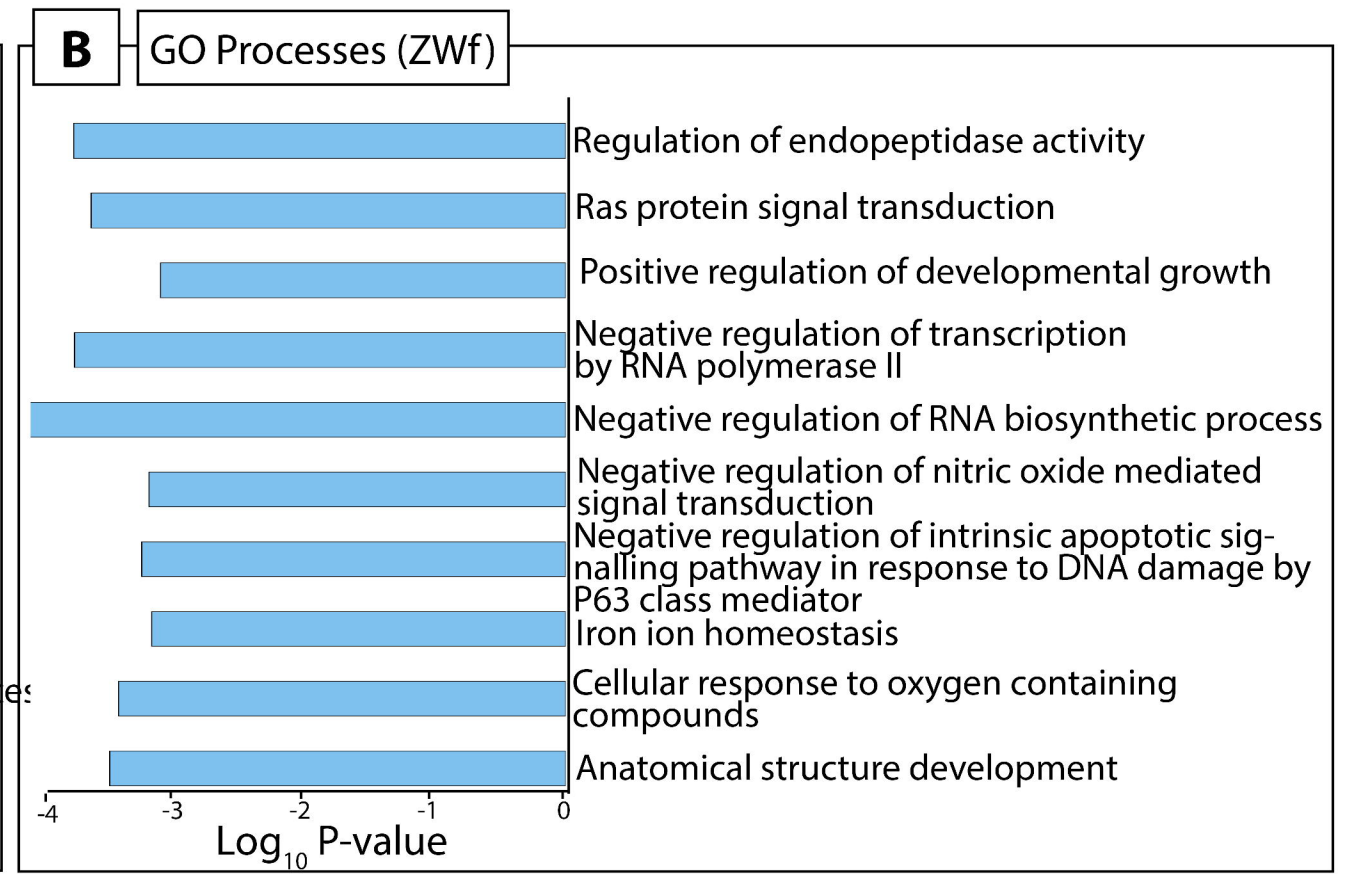

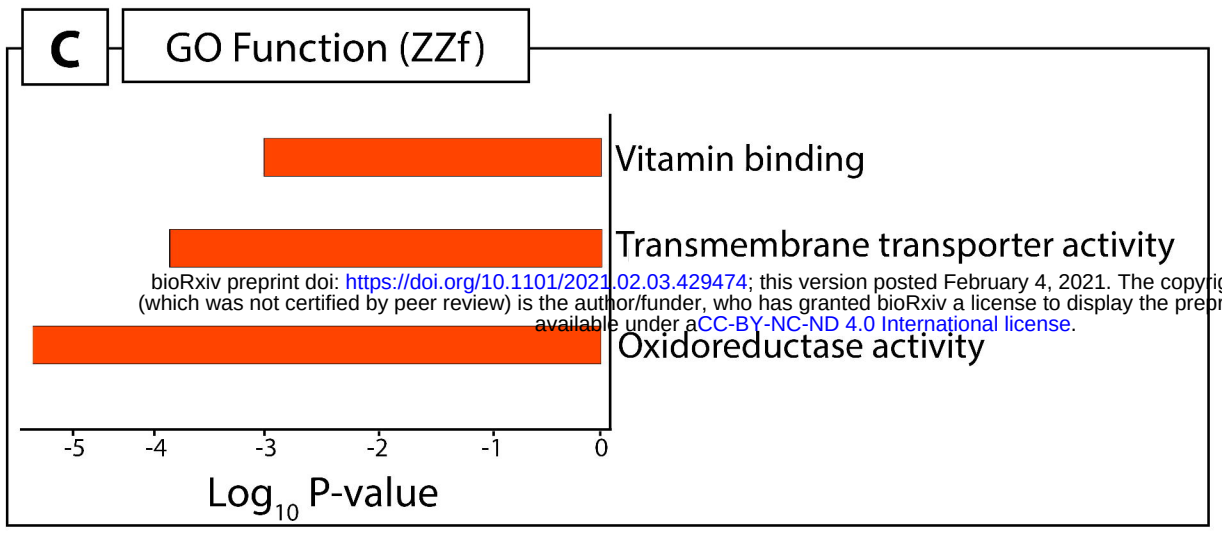

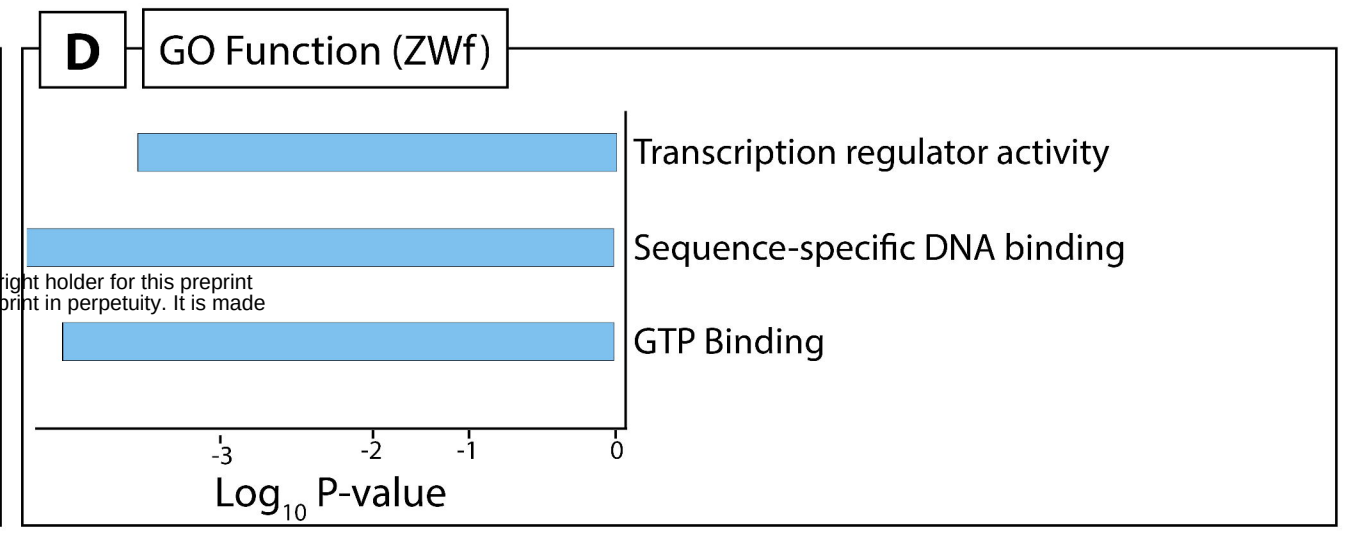

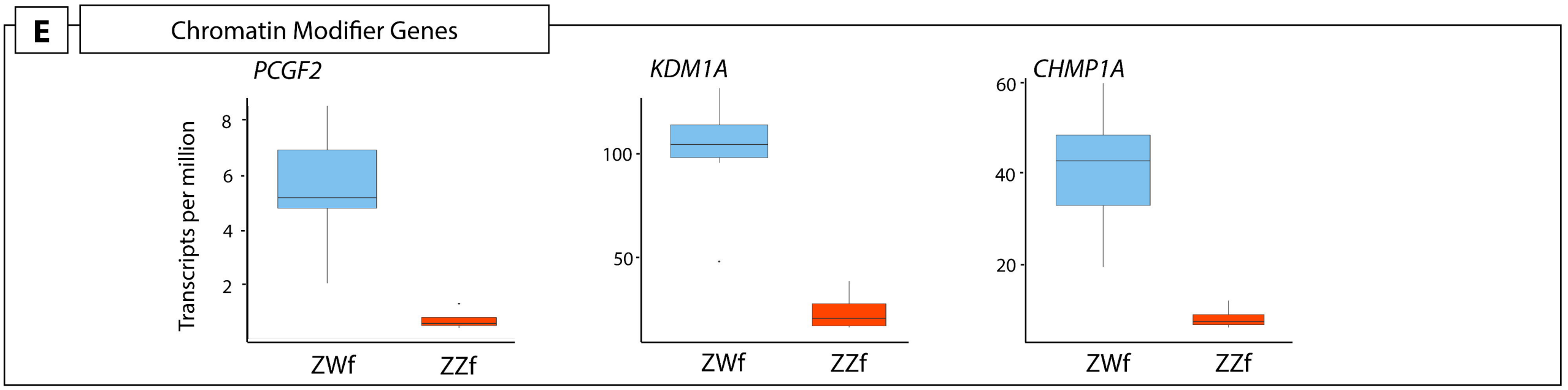

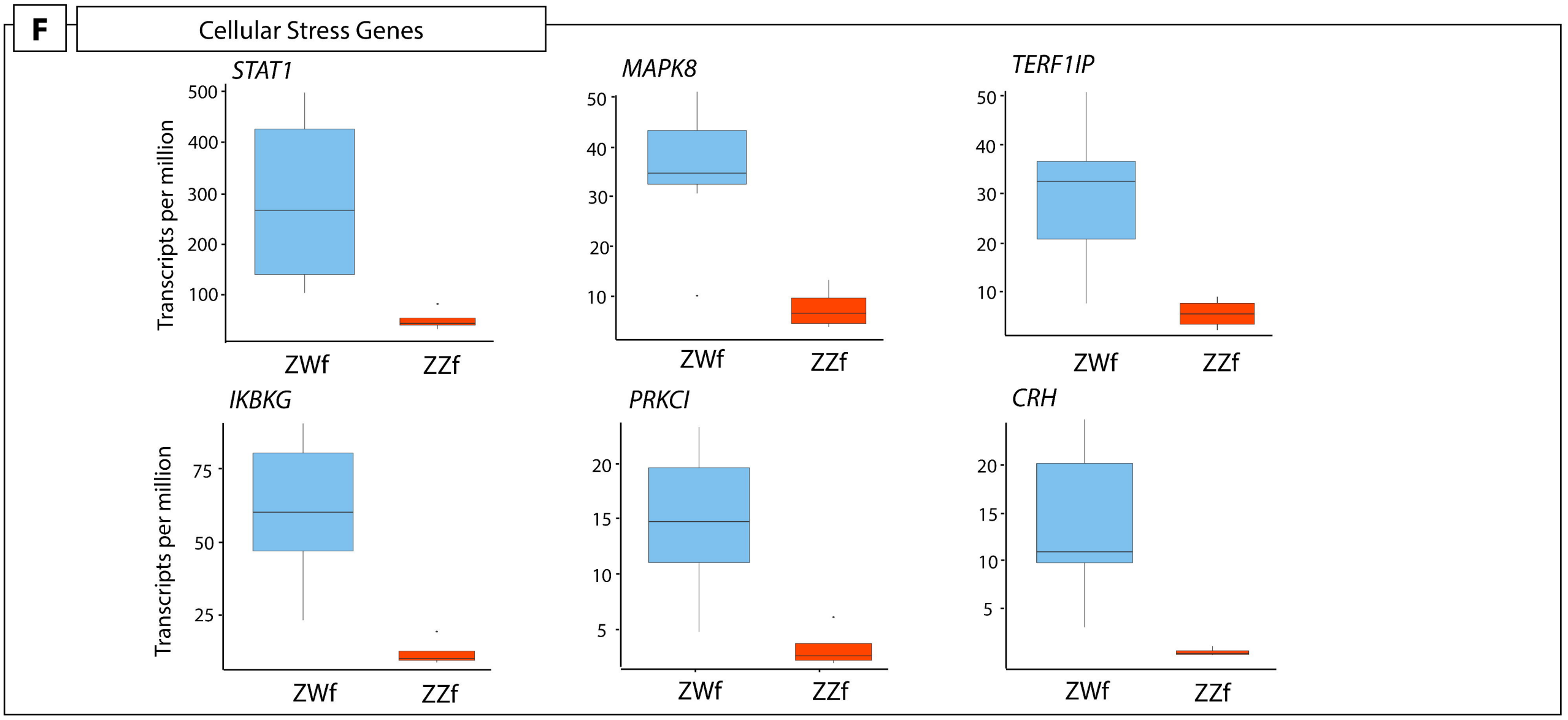

A ZZf clusters

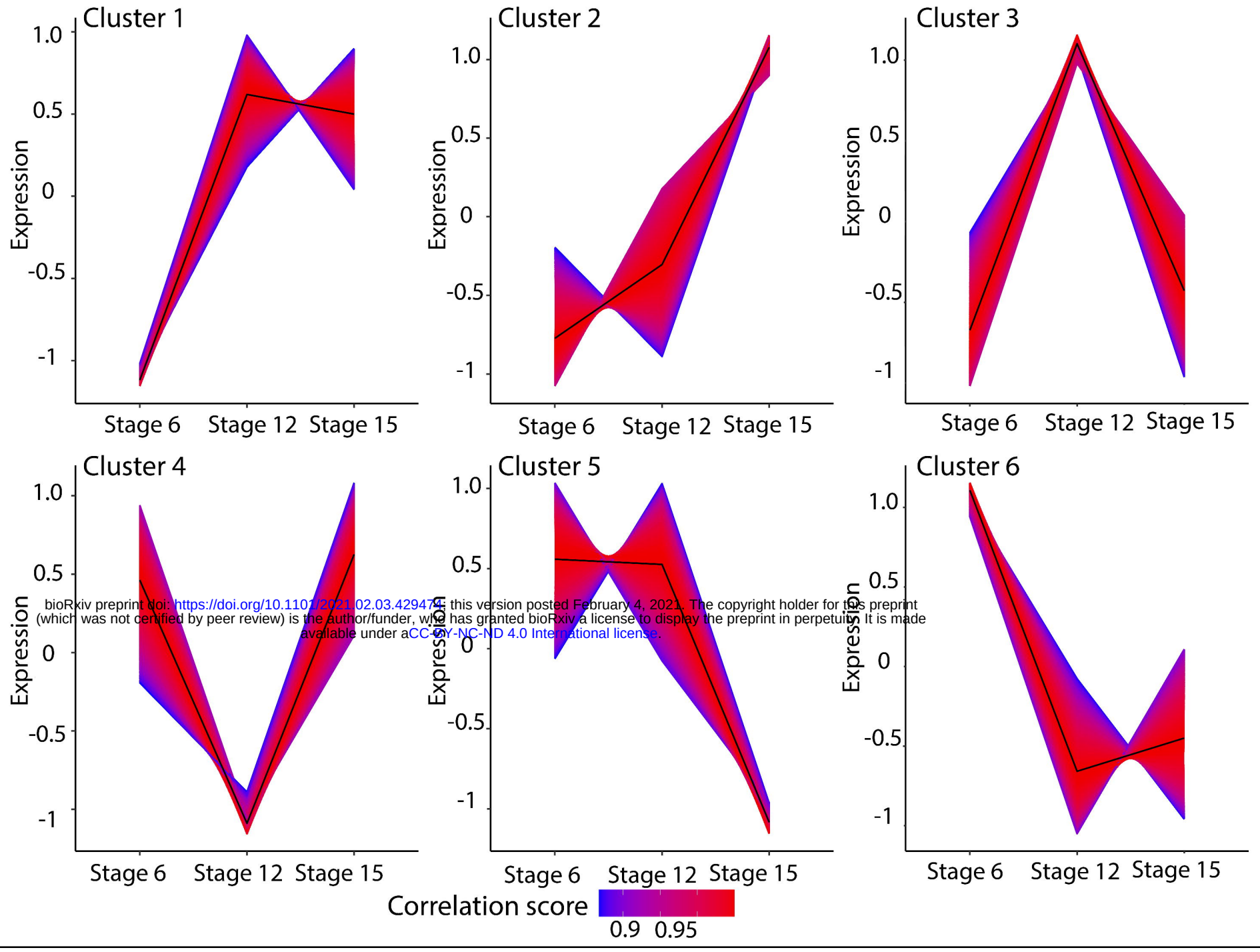

B ZWf clusters

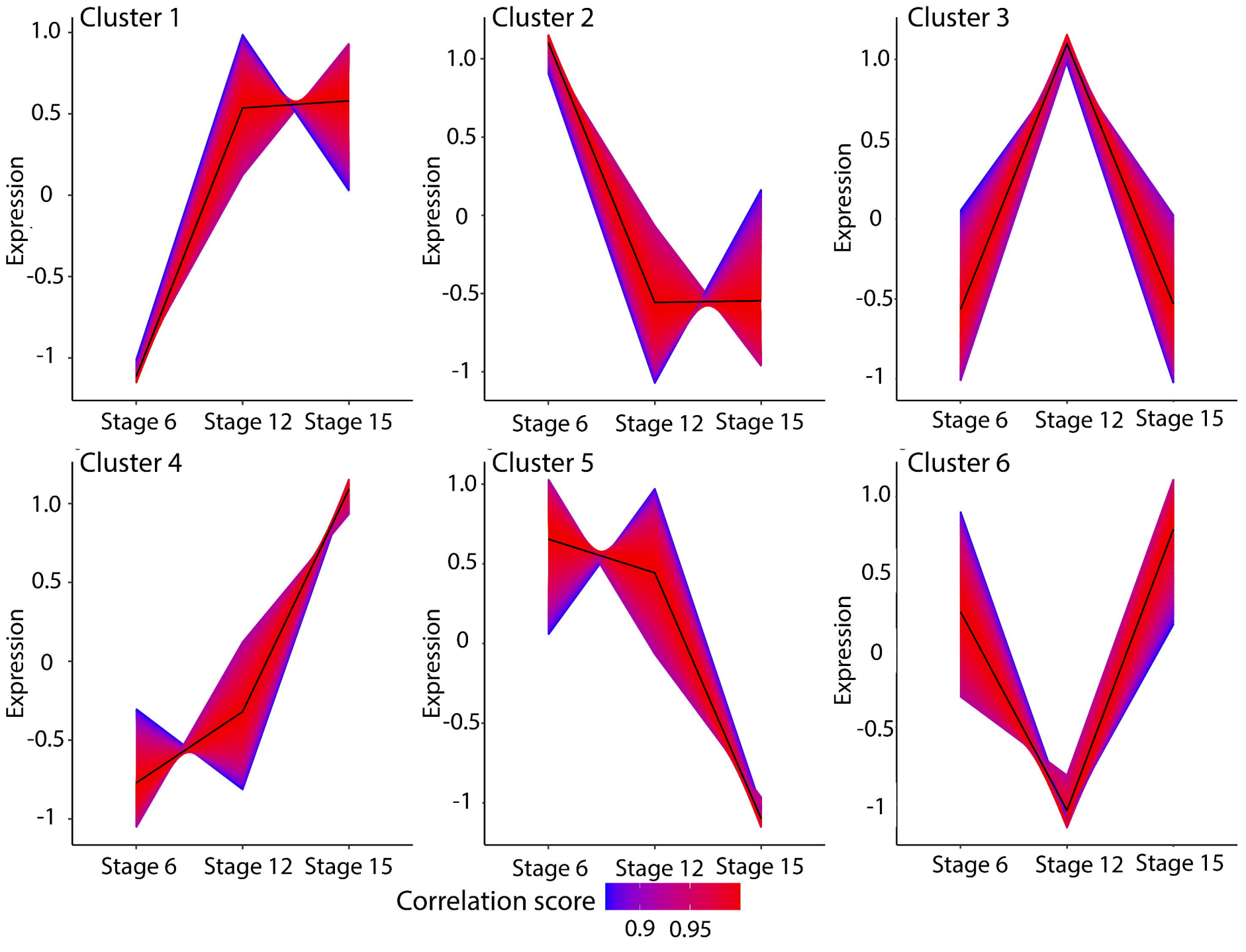

A

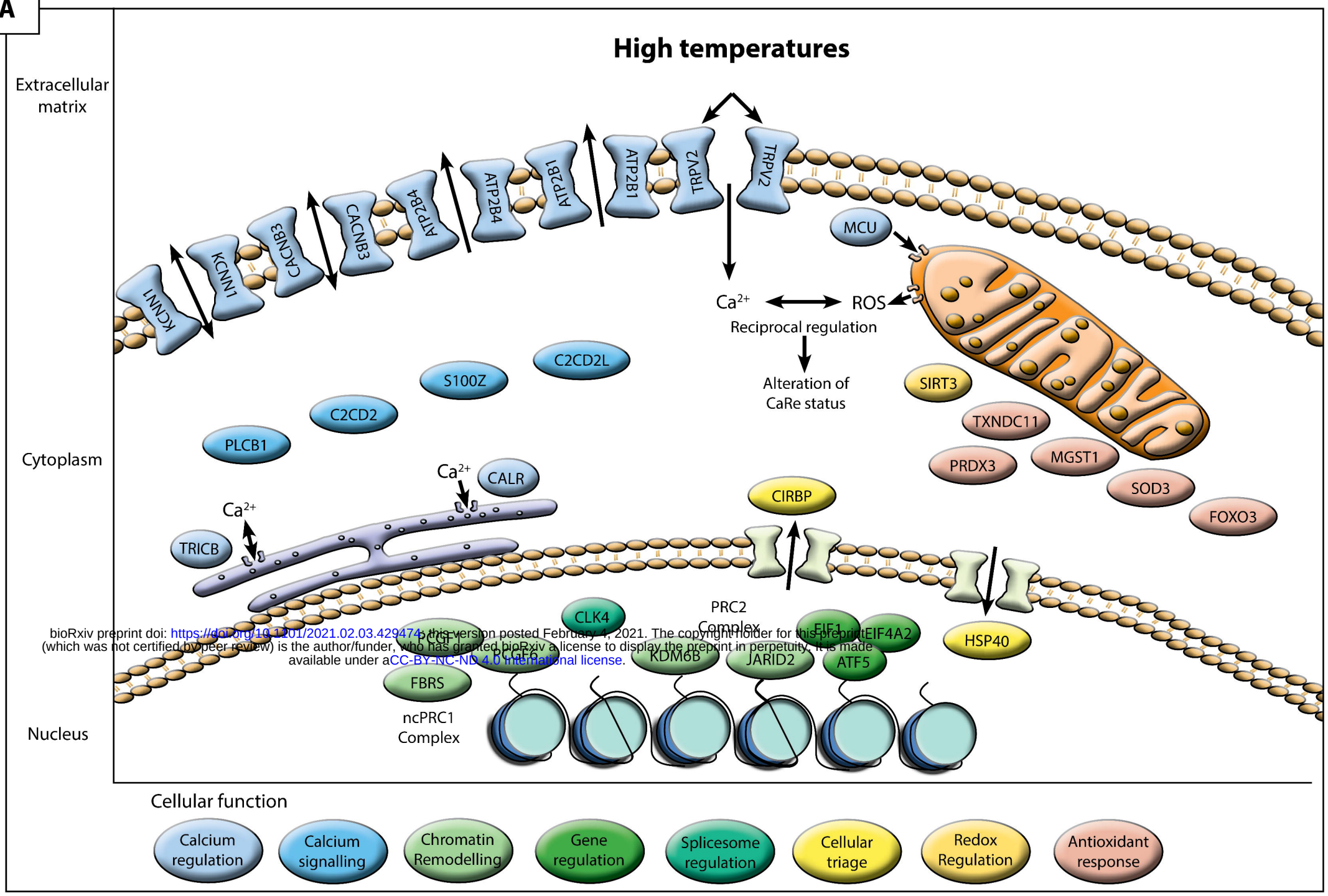

B

Gene ID	Gene Name	logFC	logCPM	F	P-Value	FDR
ATF5	Activating transcription factor 5	2.075	6.445	20.868	8.20E-5	3.42E-3
ATP2B1	ATPase plasma membrane Ca^{2+} transporting 1	1.162	5.455	24.183	3.09E-5	2.13E-3
ATP2B4	ATPase plasma membrane Ca^{2+} transporting 4	1.561	6.369	35.685	1.63E-6	4.31E-4
C2CD2	C2 calcium dependent domain containing 2	1.320	4.706	26.474	1.64E-5	1.60E-3
C2CD2L	C2CD2 like	1.330	3.288	17.857	2.12E-4	5.71E-3
CACNB3	Calcium voltage-gated channel auxiliary subunit beta 3	1.541	7.079	44.339	2.50E-7	1.69E-4
CALR	Calreticulin	1.397	9.378	23.407	3.86E-5	2.37E-3
CIRBP	Cold inducible RNA binding protein	1.166	9.763	41.691	4.32E-7	2.29E-4
CLK4	CDC like kinase 4	1.330	5.681	19.118	1.41E-4	4.47E-3
DNAJC28	DnaJ heat shock protein family (Hsp40) member C28	1.252	3.039	15.643	4.44E-4	8.72E-3
EIF1	Eukaryotic translation initiation factor 1	1.176	8.435	17.443	2.43E-4	6.11E-3
EIF4A2	Eukaryotic translation initiation factor 4A2	1.168	8.158	59.491	1.53E-8	2.87E-5
FBRS	Fibrosin	1.153	8.243	30.247	6.08E-6	8.95E-4
FOXO3	Forkhead box O3	1.129	5.798	18.598	1.67E-4	4.88E-3
JARID2	Jumonji and AT-rich interaction domain containing 2	2.296	8.620	40.274	5.85E-7	2.57E-4
KCNN1	Potassium calcium-activated channel subfamily N member 1	1.164	5.594	15.939	4.01E-4	8.21E-3
KDM6B	Lysine demethylase 6B	3.503	9.291	120.703	6.40E-12	1.08E-7
MCU	Mitochondrial calcium uniporter	1.018	5.466	26.624	1.57E-5	1.56E-3
MGST1	Microsomal glutathione S-transferase 1	1.351	7.830	29.858	6.71E-6	9.47E-4
PCGF1	Polycomb group ring finger 1	1.408	5.170	19.275	1.34E-4	4.42E-3
PCGF6	Polycomb group ring finger 6	1.072	4.330	19.318	1.33E-4	4.39E-3
PLCB1	Phospholipase C beta 1	1.763	3.649	24.040	3.22E-5	2.17E-3
PRDX3	Peroxiredoxin 3	1.336	7.212	29.894	6.65E-6	9.46E-4
S100Z	S100 calcium binding protein Z	4.202	3.813	23.471	3.79E-5	2.37E-3
SIRT3	Sirtuin 3	1.264	2.359	18.039	2.00E-4	5.52E-3
SOD3	Superoxide dismutase 3	2.317	1.806	17.239	2.59E-4	6.33E-3
TMEM38B	Transmembrane protein 38B	1.437	3.311	26.252	1.74E-5	1.62E-3
TRPV2	Transient receptor potential cation channel subfamily V member 2	3.239	3.951	45.162	2.12E-7	1.49E-4
TXNDC11	Thioredoxin domain containing 11	1.024	6.160	23.816	3.43E-5	2.26E-3

A

ZZf vs ZWf at each stage

Stage 6

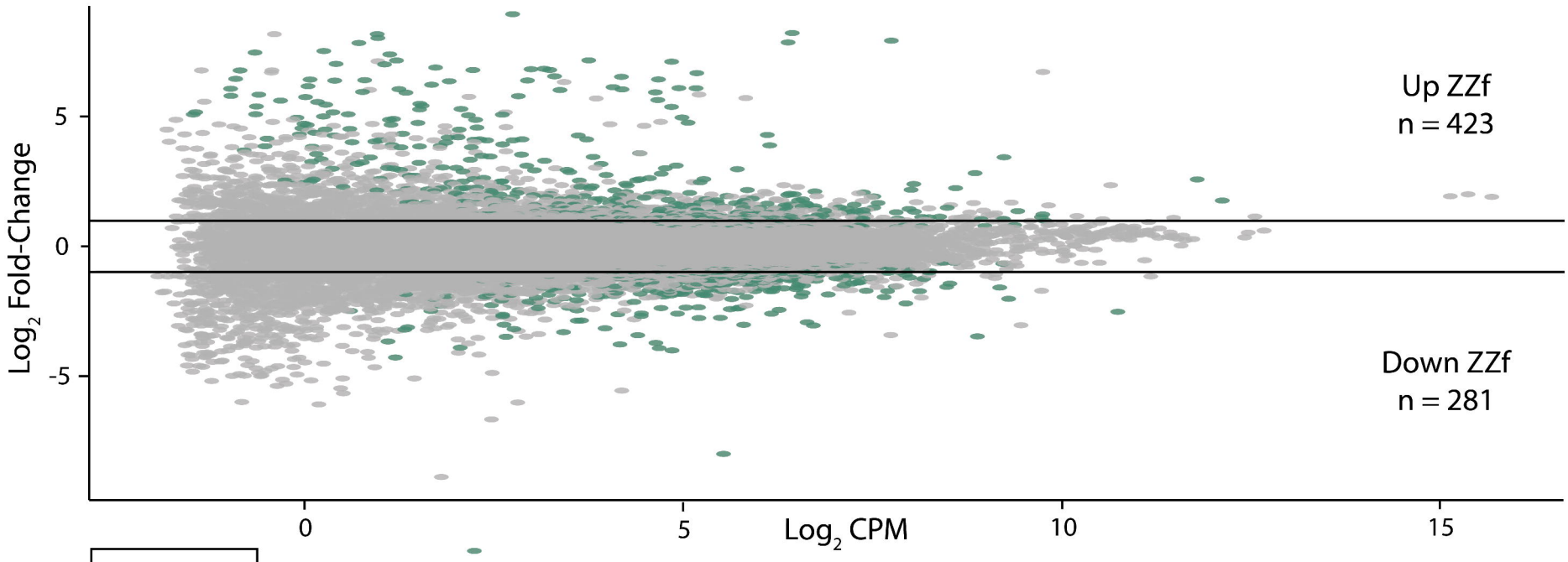

Stage 12

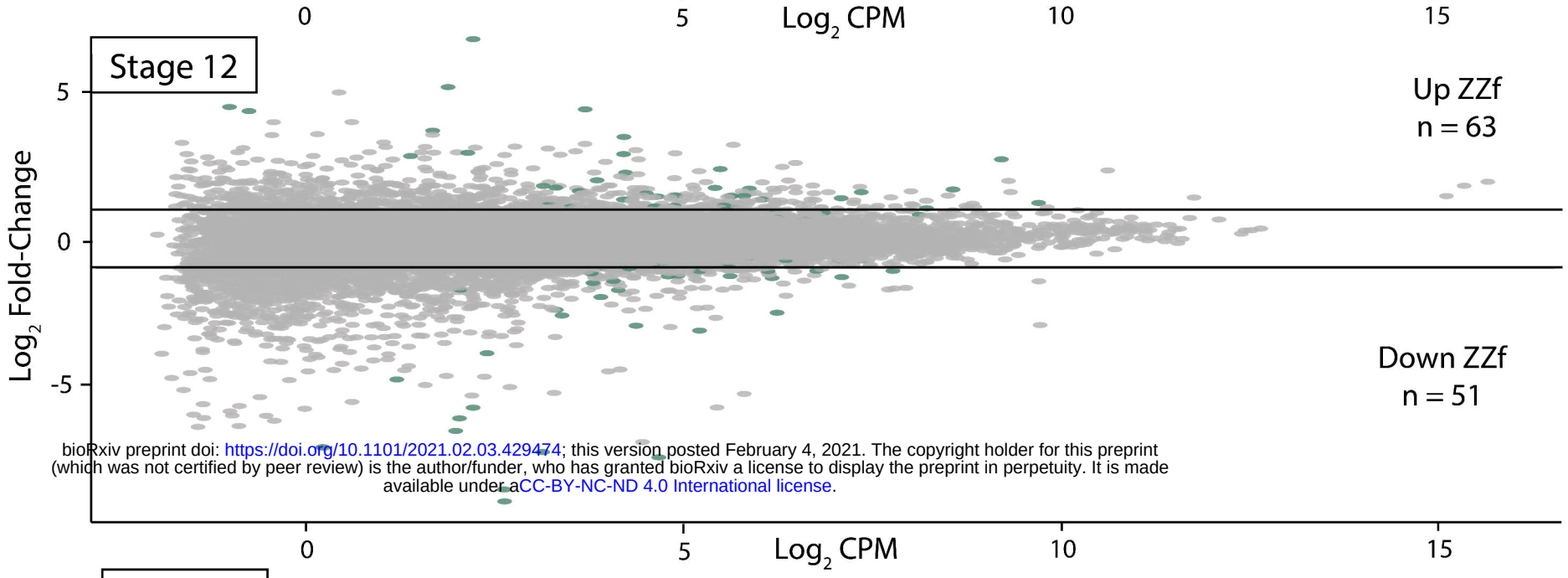

Stage 15

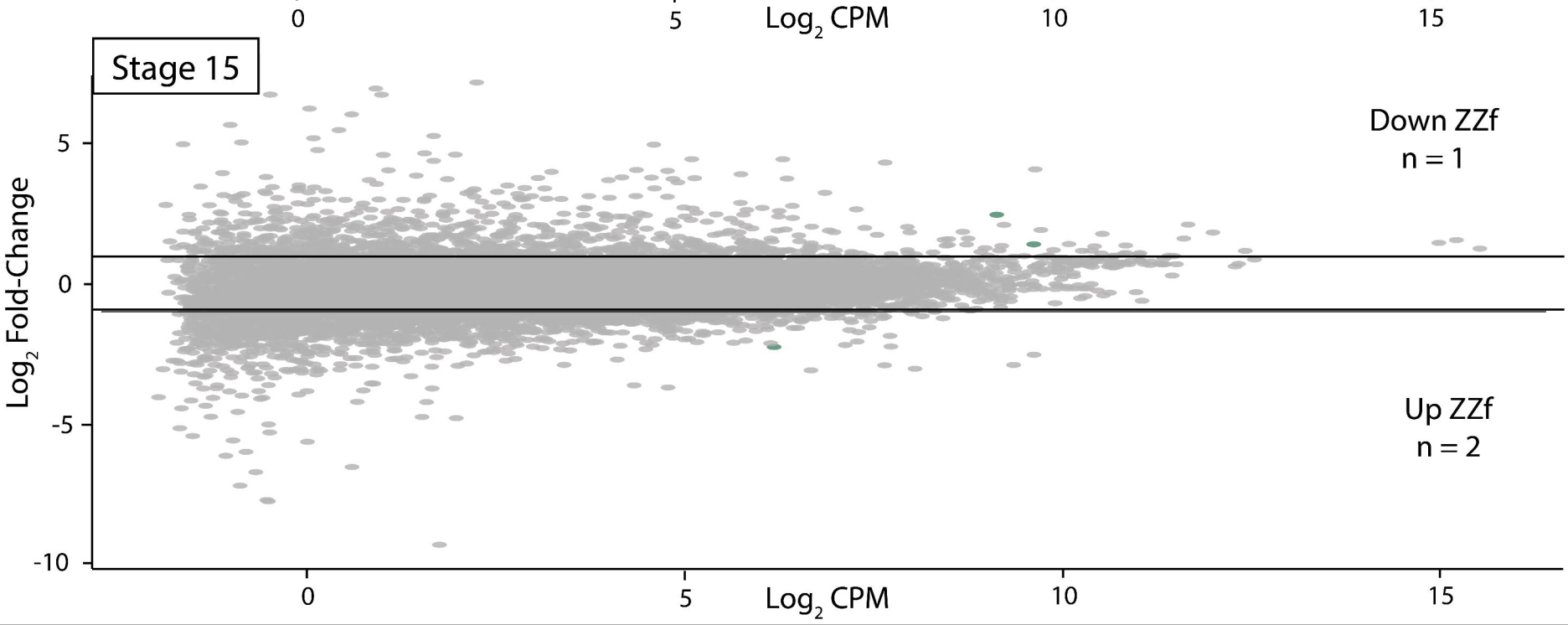

B

Between stage comparisons

ZZf: Stage 6 vs 12

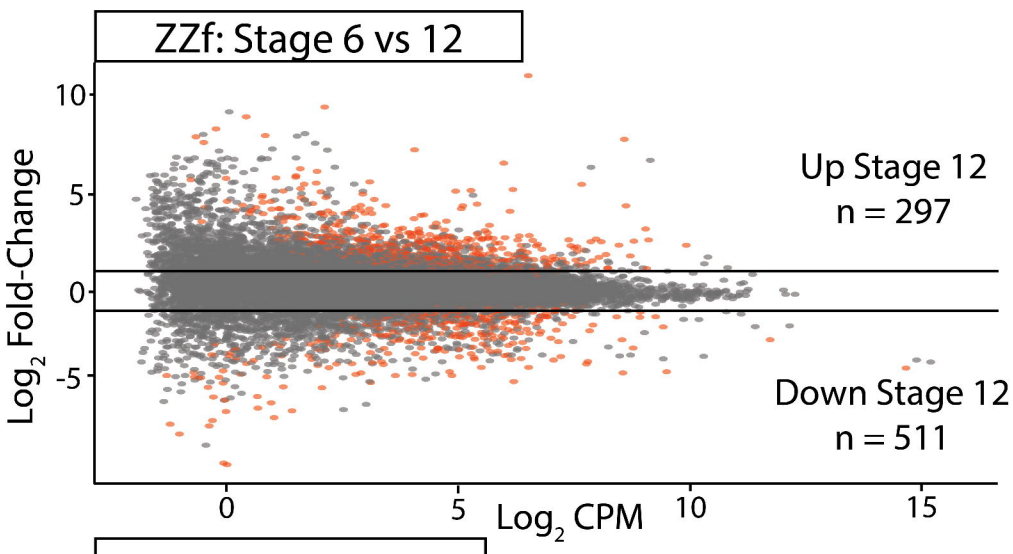

ZWf: Stage 6 vs 12

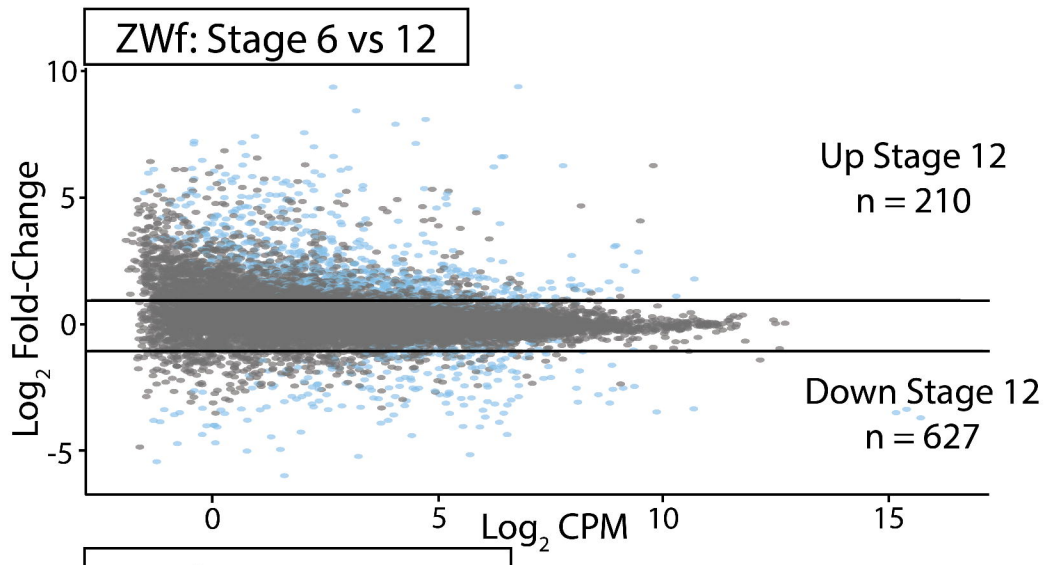

ZZf: Stage 12 vs 15

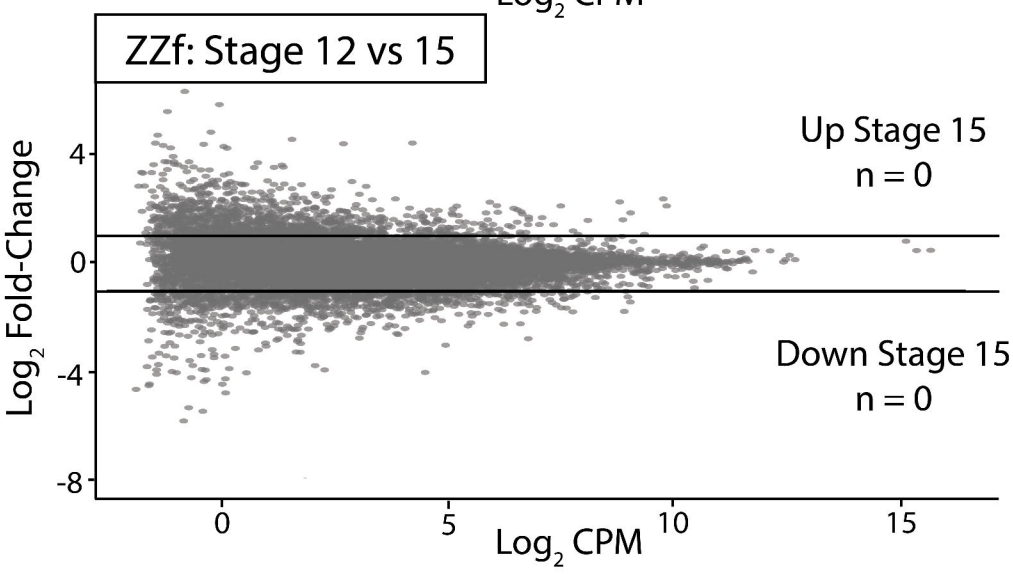

ZWf: Stage 12 vs 15

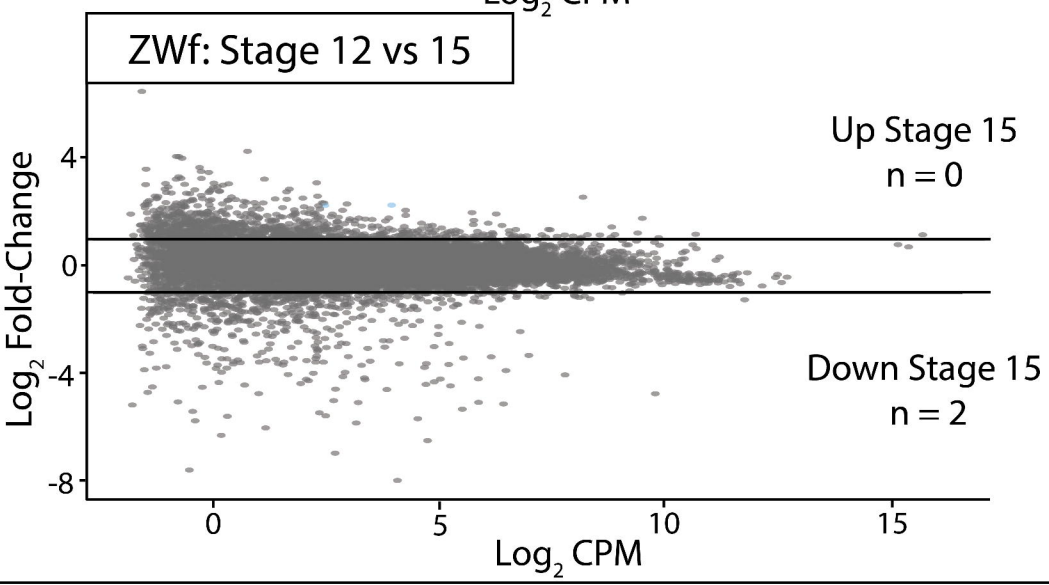

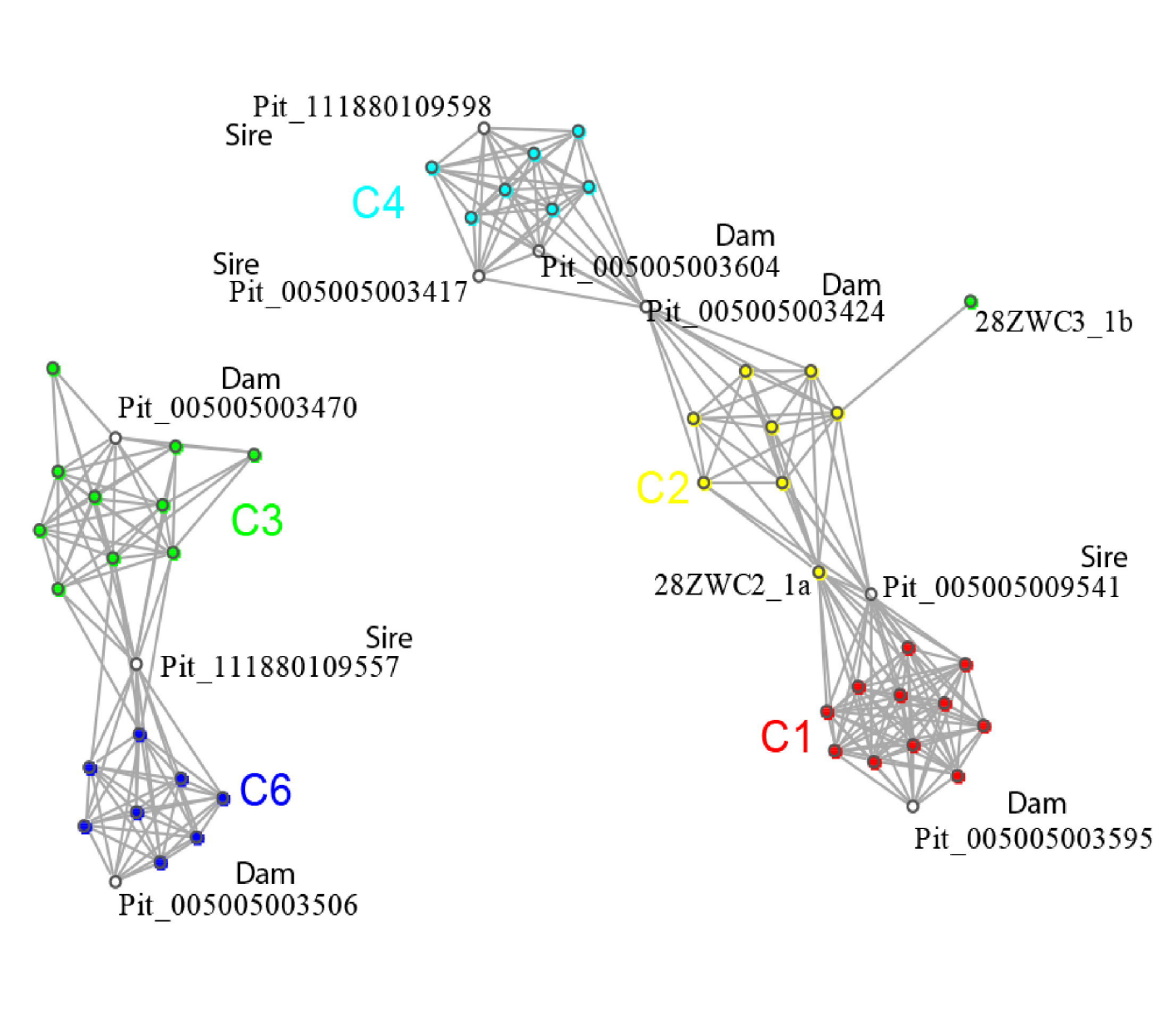
Pit_111880109598
Sire
C4
Dam
Pit_005005003604
Sire
Pit_005005003417
Dam
Pit_005005003424
28ZWC3_1b
Dam
Pit_005005003470
C3
C2
Sire
28ZWC2_1a
Pit_005005009541
Sire
Pit_111880109557
C1
C6
Dam
Pit_005005003595
Dam
Pit_005005003506

A Female Gene Panel

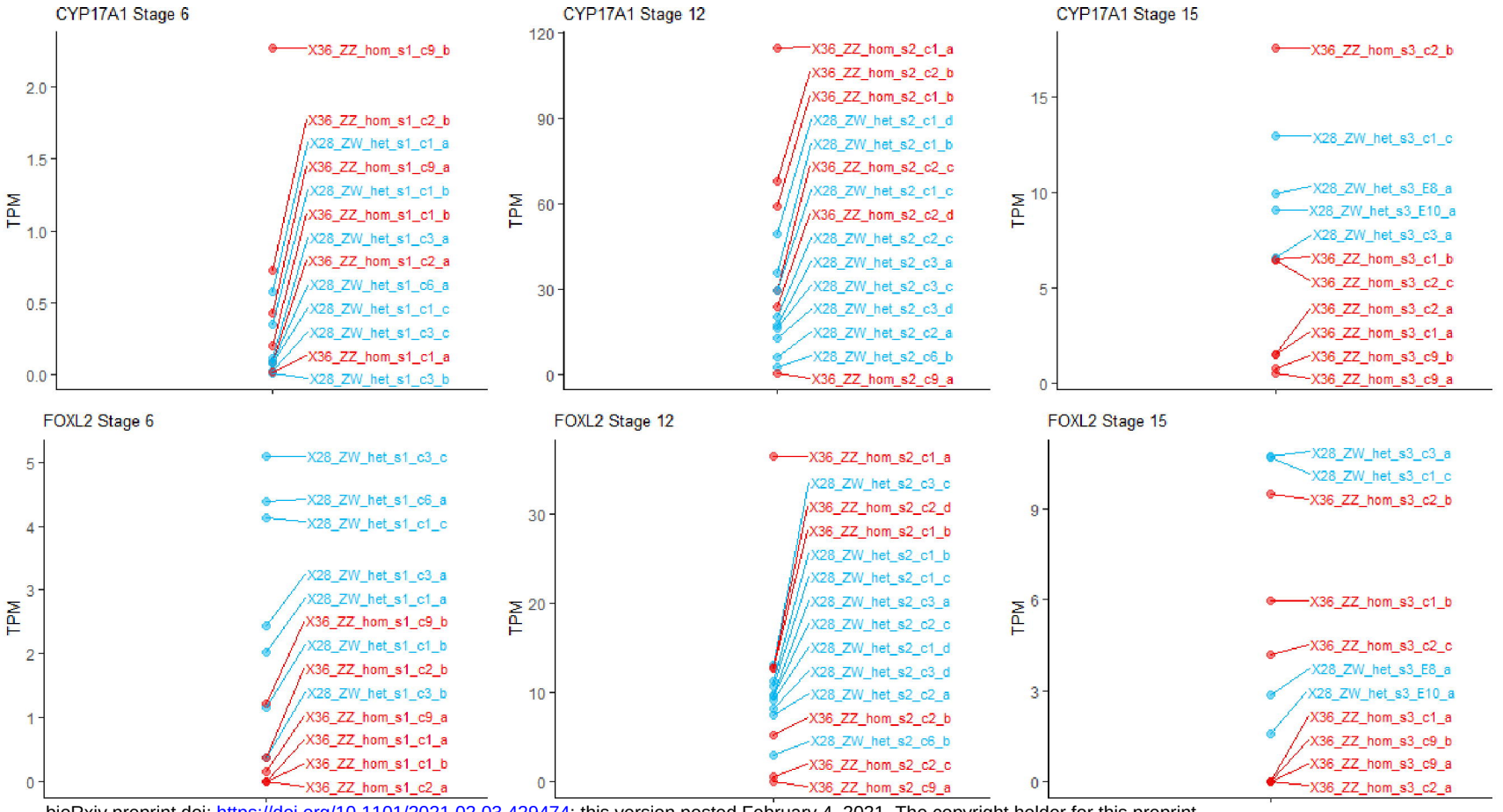

B Male Gene Panel

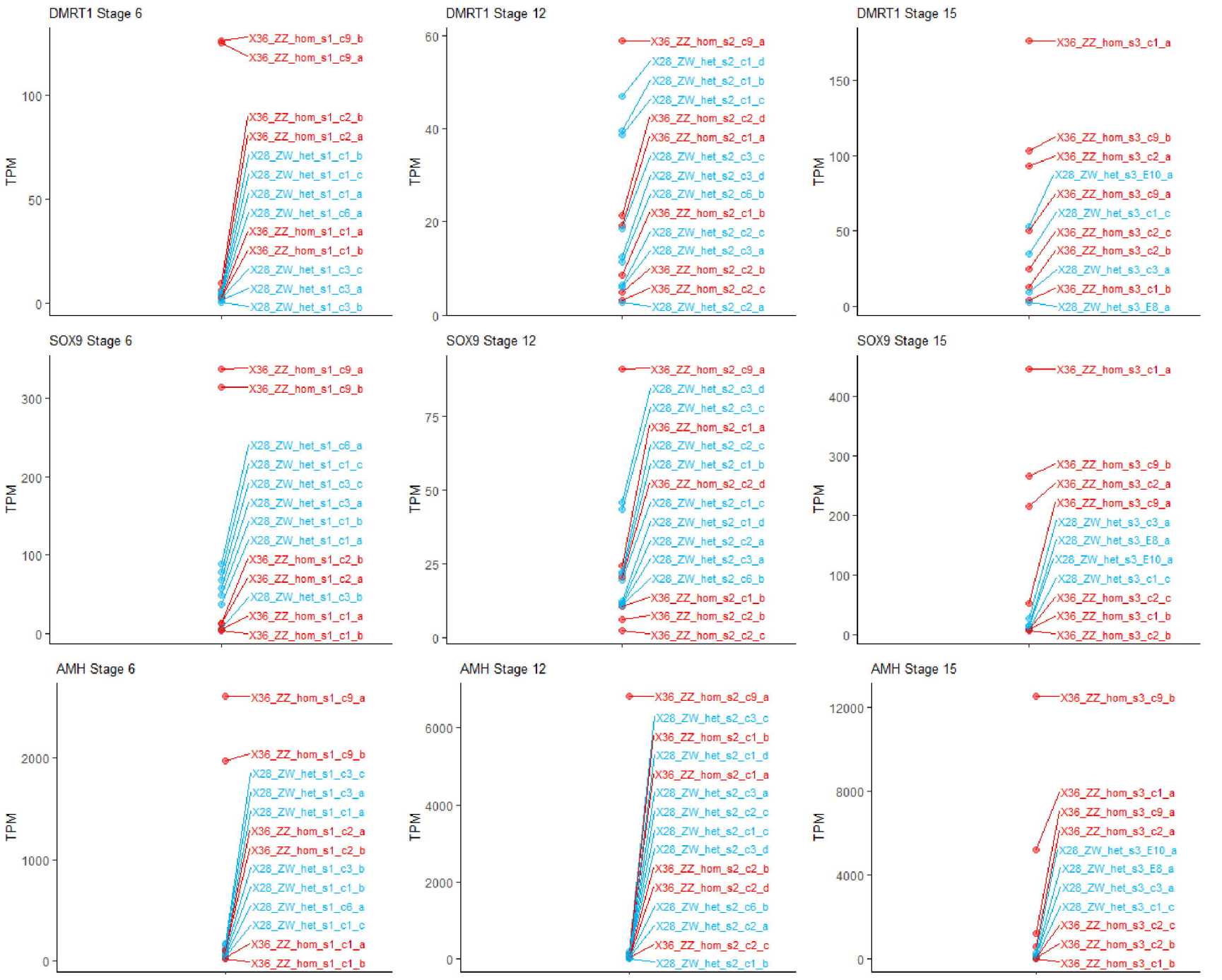

A All Samples

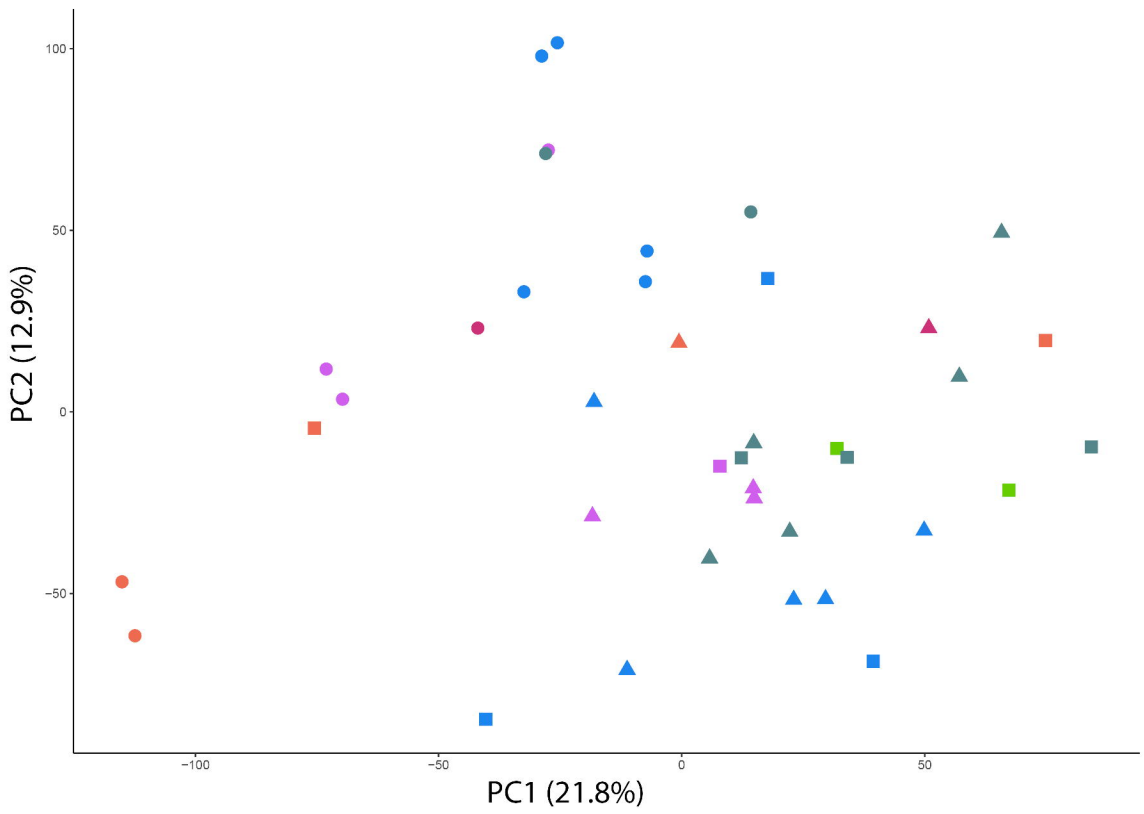

B Clutch 9 Removed

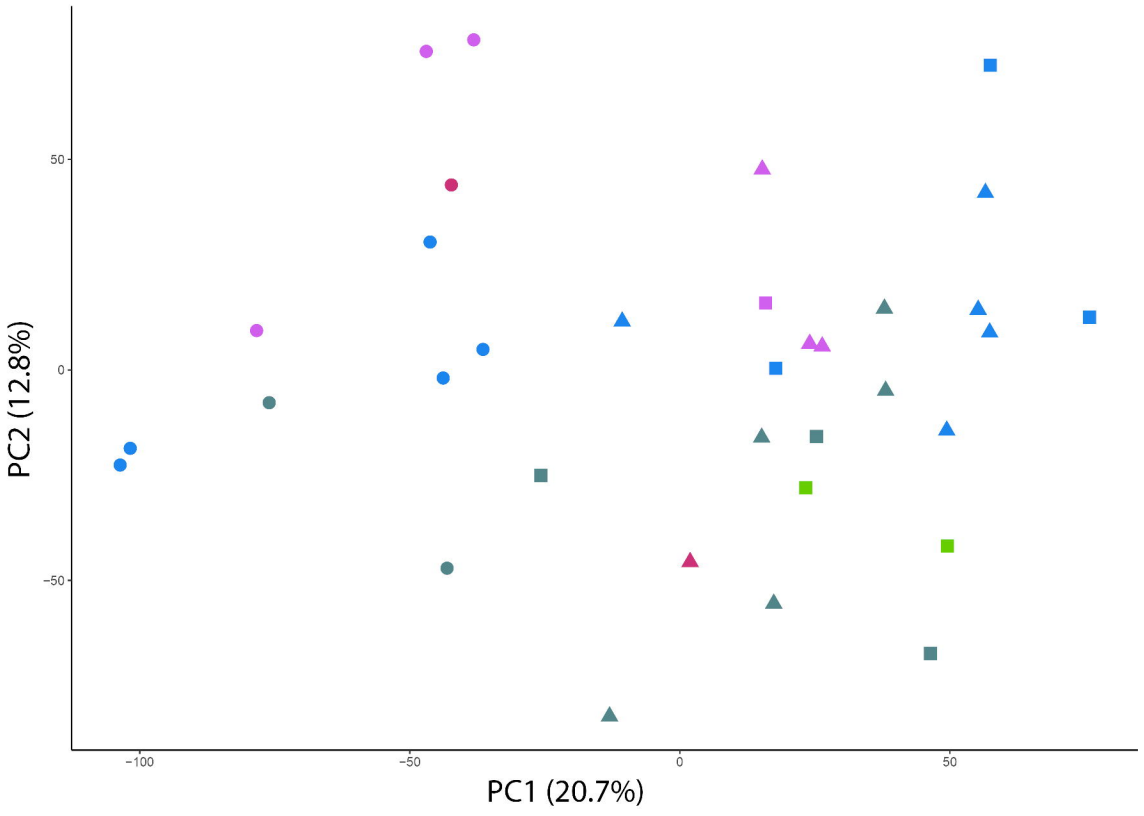

C Non-Sex Reversed Removed

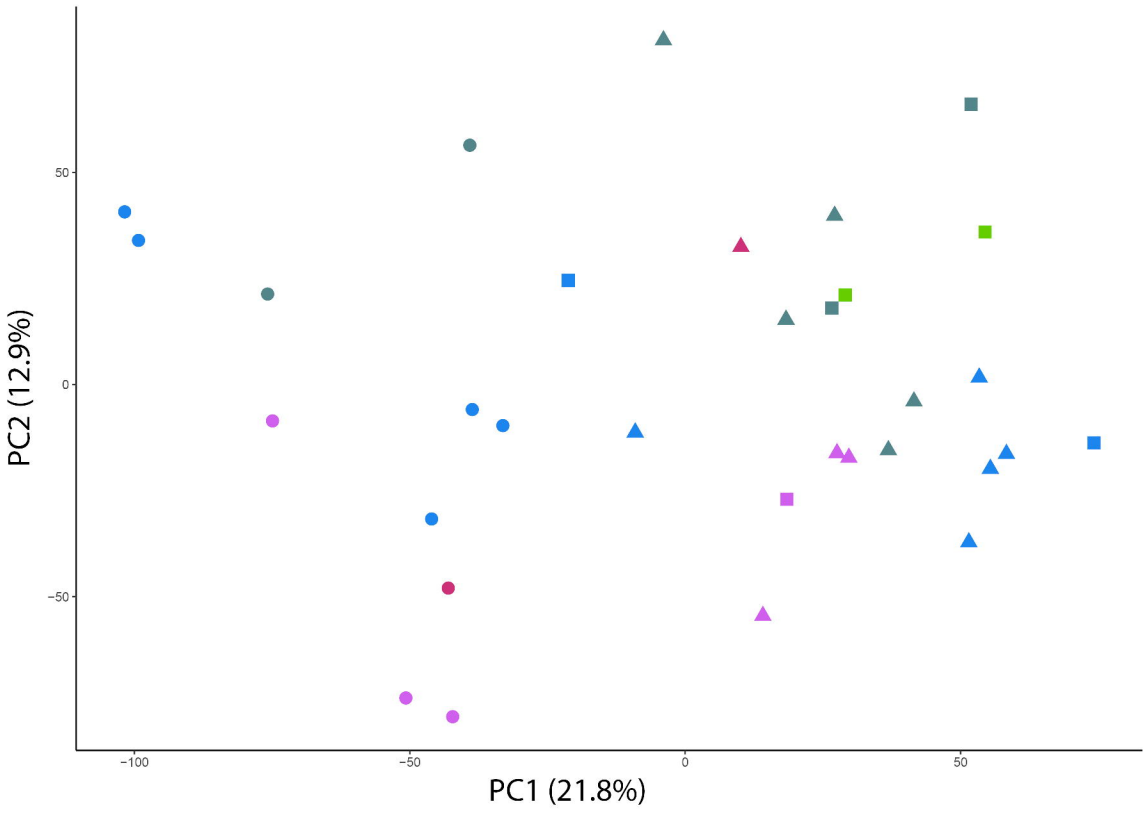

Legend

Stage 6 Stage 12 Stage 15

Clutch 1 Clutch 2 Clutch 3 Clutch 6 Clutch 9 Clutch 10